CANCER

A conserved long-distance telomeric silencing mechanism suppresses mTOR signaling in aging human fibroblasts

Kathrin Jäger[1,2], Juliane Mensch[1,2], Maria Elisabeth Grimmig[1], Bruno Neuner[3], Kerstin Gorzelniak[4], Seval Türkmen[5,6], Ilja Demuth[7,8], Alexander Hartmann[1], Christiane Hartmann[9], Felix Wittig[10], Anje Sporbert[11], Andreas Hermann[9,12,13], Georg Fuellen[14], Steffen Möller[14], Michael Walter[1,2]*

Telomeres are repetitive nucleotide sequences at the ends of each chromosome. It has been hypothesized that telomere attrition evolved as a tumor suppressor mechanism in large long-lived species. Long telomeres can silence genes millions of bases away through a looping mechanism called telomere position effect over long distances (TPE-OLD). The function of this silencing mechanism is unknown. We determined a set of 2322 genes with high positional conservation across replicatively aging species that includes known and candidate TPE-OLD genes that may mitigate potentially harmful effects of replicative aging. Notably, we identified *PPP2R2C* as a tumor suppressor gene, whose up-regulation by TPE-OLD in aged human fibroblasts leads to dephosphorylation of p70S6 kinase and mammalian target of rapamycin suppression. A mechanistic link between telomeres and a tumor suppressor mechanism supports the hypothesis that replicative aging fulfills a tumor suppressor function and motivates previously unknown antitumor and antiaging strategies.

INTRODUCTION

Telomeres are repetitive nucleotide sequences that protect the natural ends of linear chromosomes (*1*). The exact role of telomeres in aging is still a matter of debate. Successive telomere attrition during cell divisions provides a molecular mechanism that determines replicative life span (*1*, *2*), which ultimately leads to cellular senescence. Telomere shortening was proposed to be a tumor suppressor mechanism a long time ago (*2*, *3*). Successive telomere attrition during replication (*4*) eventually triggers the DNA damage response when telomeres become critically shortened, leading to cell cycle arrest and replicative senescence. It is believed that this mechanism acts as a tumor suppressor mechanism in humans and other large, long-lived species (*2*) at the cost of possible negative effects in later life (*5*). Clinical observations support this concept as most clinically detectable cancers have reactivated telomerase (*1*). Nevertheless, there is still much controversy about the functional and physiological role of replicative aging. A main reason is the double-edged role of telomere attrition (*6*). Excessive shortening of the telomere is itself tumorigenic. Short telomeres are found in premalignancies and may increase genetic instability and tumor formation in mice (*7*).

In 2001, a process called telomere position effect (TPE), i.e., the reversible silencing of telomeric genes, was demonstrated in human HeLa cells using a luciferase reporter (*8*). Together, 16 genes were identified using cultivated myoblasts and fibroblasts, which are differentially expressed in young cells (with long telomeres) versus old cells (with short telomeres). Most of these genes are silenced in young cells (with long telomeres) and become expressed when telomeres are short (table S1). Re-elongation of telomeres in cells with short telomeres by exogenous expression of the h*TERT* gene (active telomerase) results in expression patterns similar to those in young cells with long telomeres (*9*, *10*). As the silencing mechanism acts via looping structures up to at least 15 Mb away from the telomere, as experimentally proven for the five genes, *C1S*, *DSP*, *ISG15* (*10*, *11*), *SORBS2* (*9*), and *hTERT* (*12*), it was named telomere position effect over long distance (TPE-OLD) (Fig. 1A). Not much is known about the functional details of TPE-OLD. The ability to regulate genes by telomere length (TL) in a preemptive fashion, e.g., without induction of a strong DNA damage signal from critically short telomeres, may have important implications for the regulation of subtle age-dependent adjustments, which prompted us to study these interrelationships in more detail.

We used a bioinformatics approach to identify TPE-OLD candidate genes and investigated gene expression of candidates in human fibroblasts at high population doublings (PDs) (with short telomeres) and in h*TERT* immortalized fibroblasts (with long telomeres). Fibroblasts from patients with Hutchinson-Gilford progeria (HGP) were used as a model for accelerated telomere attrition. HGP cells display

[1]Institute of Clinical Chemistry and Laboratory Medicine, Rostock University Medical Center, University of Rostock, Rostock, Germany. [2]Charité–Universitätsmedizin Berlin, corporate member of Freie Universität Berlin, Humboldt-Universität zu Berlin, and Berlin Institute of Health, Institute of Laboratory Medicine, Clinical Chemistry and Pathobiochemistry, Berlin, Germany. [3]Charité–Universitätsmedizin Berlin, corporate member of Freie Universität Berlin, Humboldt-Universität zu Berlin, and Berlin Institute of Health, Department of Anesthesiology and Intensive Care Medicine, Berlin, Germany. [4]Unfallkrankenhaus Berlin, Institute of Laboratory Medicine, Berlin, Germany. [5]LNS Hematooncogenetics, National Center of Genetics Luxembourg, Dudelange, Luxemburg. [6]Charité–Universitätsmedizin Berlin, corporate member of Freie Universität Berlin, Humboldt-Universität zu Berlin, and Berlin Institute of Health, Institute of Medical Genetics and Human Genetics, Berlin, Germany. [7]Charité–Universitätsmedizin Berlin, corporate member of Freie Universität Berlin, Humboldt-Universität zu Berlin, and Berlin Institute of Health, Department of Endocrinology and Metabolism, Berlin, Germany. [8]Berlin Institute of Health at Charité–Universitätsmedizin Berlin, BCRT - Berlin Institute of Health Center for Regenerative Therapies, Berlin, Germany. [9]Translational Neurodegeneration Section "Albrecht-Kossel", Department of Neurology, Rostock University Medical Center, University of Rostock, 18147 Rostock, Germany. [10]Institute of Pharmacology and Toxicology, Rostock University Medical Center, University of Rostock, Rostock, Germany. [11]Advanced Light Microscopy, Max Delbrück Center for Molecular Medicine, Berlin, Germany. [12]Deutsches Zentrum für Neurodegenerative Erkrankungen (DZNE) Rostock/Greifswald, Rostock, Germany. [13]Center for Transdisciplinary Neurosciences Rostock (CTNR), University Medical Center Rostock, Rostock, Germany. [14]Institute for Biostatistics and Informatics in Medicine and Ageing Research, Rostock University Medical Center, Rostock, Germany.
*Corresponding author. Email: michael.walter@med.uni-rostock.de

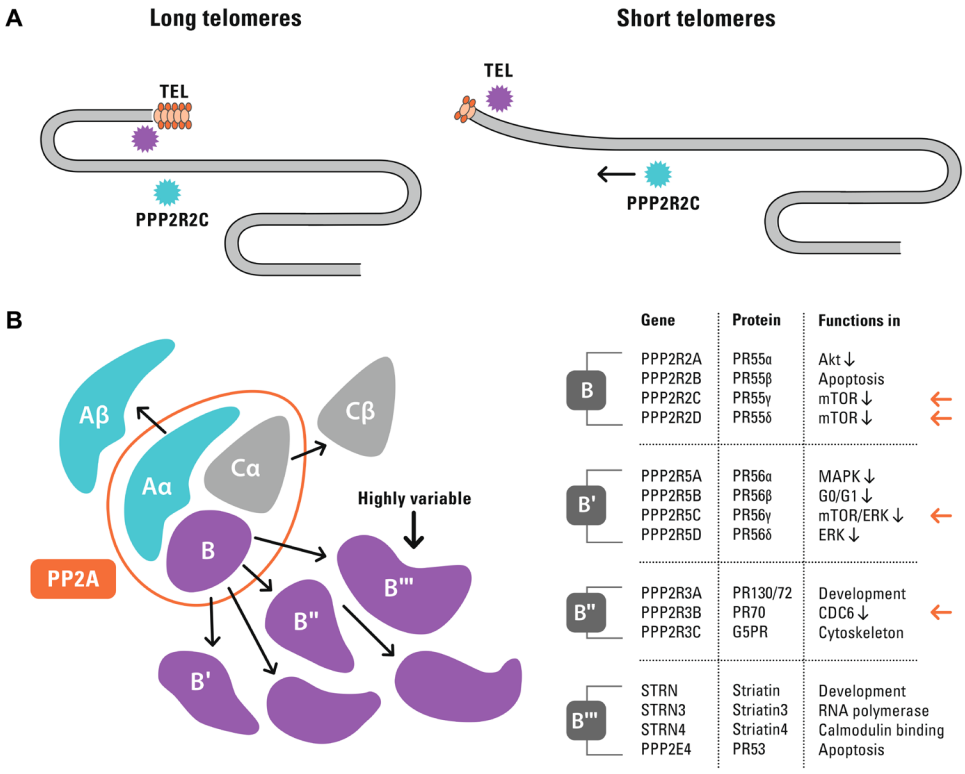

Fig. 1. TPE-OLD concept and protein phosphatase 2A holoenzyme subunits as TPE-OLD candidates. (**A**) TPE-OLD concept. Telomeres may loop to specific loci to regulate gene expression, a process termed "telomere position effect over long distances" (*9*, *10*, *12*). The effect extends to a distance of at least 15 Mb from the telomere and may regulate gene expression in an age-dependent manner. (**B**) Schematic representation of the structural (Aα and Aβ), regulatory (B, B′, B″, and B‴) and catalytic (Cα and Cβ) subunits forming the PP2A holoenzyme. The enzyme is composed of one of two homologous catalytic subunits, one of two homologous structural subunits, and 1 of at least 15 highly variable regulatory subunits. The included table summarizes functional roles of the regulatory subunits. Red arrows indicate the TPE-OLD candidates, all displaying similar regulatory functions, as indicated by (*21*–*24*). MAPK, mitogen-activated protein kinase; ERK, extracellular signal–regulated kinase.

shorter telomeres and abnormal TL distribution (*13*, *14*). Patients with HGP show many phenomena of normal aging at young age but a low cancer incidence and no age-related neurodegeneration (*15*). We identified 2322 TPE-OLD candidate genes, many of which are involved in cell cycle control, metabolic regulation, and stress response. We used one of these candidates (*PPP2R2C*) to show a mechanistic link between telomere attrition and a tumor suppressor mechanism that acts long before telomere-driven DNA damage signaling occurs, driving a tumor suppressor effect based on attenuated mammalian target of rapamycin (mTOR) signaling. *PPP2R2C* encodes PR55γ, a regulatory subunit of the serine/threonine-specific phosphatase (PP2A) with a wide variety of substrates involved in the regulation of cell cycle and metabolism (Fig. 1B) (*16*, *17*). Our findings suggest an important functional role of TPE-OLD in aging cells and support the hypothesis that replicative aging fulfills a tumor suppressor function.

RESULTS

Genomic positional conservation analysis identifies previously unidentified TPE-OLD candidate genes

We first sought to identify candidate genes that might be affected by TPE-OLD by using a bioinformatics approach. Thinking in terms of biological mechanisms, most phenomena are gradual and the distinction between replicatively aging species and other species can be expected to be gradual as well. While some species are "clearly aging replicatively," this attribute is difficult to assign in many cases. When selecting the species, we therefore adopted the simplest possible definition. The criteria for categorizing a species as having "assumed TL-dependent replicative aging" were set as TL < 20 kb, undetectable telomerase levels, and no stasis (stress associated senescence), as previously proposed by Gomes *et al.* (*18*). By using these criteria, we noted that the 16 known or suggested TPE-OLD genes reported in the literature (*9*–*12*) appeared to be preserved at two telomeric positions in "replicatively aging species," that is, in species which undergo TL-dependent replicative aging (*18*), including both primates and nonprimates (at 0.2 to 7.5 Mb and at 13 to 17 Mb) (Fig. 2A and fig. S1). No such conservation was observed in organisms that do not undergo TL-dependent aging.

We used the Ensembl genome database to screen for other genes presenting a similar conserved position as this set of genes with established TPE-OLD. We selected possible candidates on the basis of positional conservation, at most 1 Mb apart, and anywhere within 17 Mb of the telomere, e.g., the maximum distance discussed in the literature for TPE-OLD effects. Using this approach, we identified 2322 novel TPE-OLD candidates (fig. S3 and table S2). Gene set enrichment analysis found that many candidates are involved in proliferation, metabolism, and stress response and/or are regulated by transcription factors involved in proliferation, metabolism, development, and response to stress and DNA damage (table S3) (*19*, *20*). Accordingly, gene families associated with transcriptional regulation,

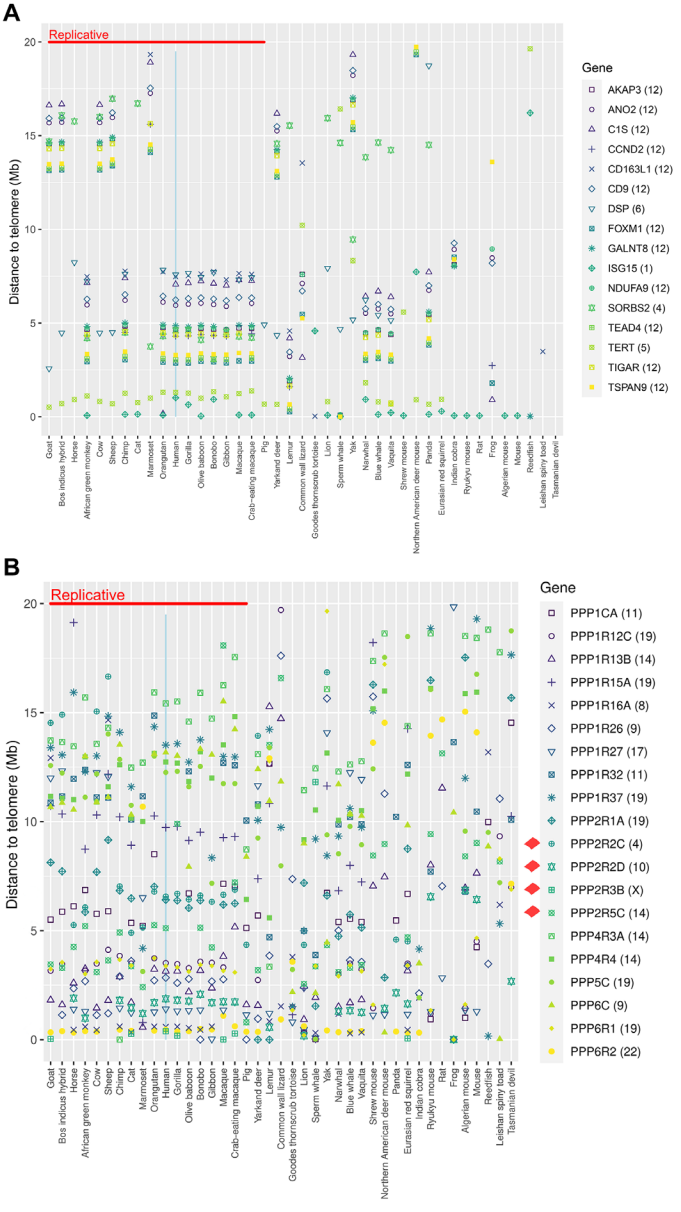

Fig. 2. Conserved genomic positions of known TPE-OLD genes and identification of TPE-OLD candidate genes encoding PP2A subunits. (**A**) Telomeric distances for established TPE-OLD genes. The figure shows the distance to the closest telomere in megabases for all genes for which a TPE-OLD was already proposed in the literature, capped at 20 Mb. Genes are distinguished by their symbol, supported by color. Species are separated horizontally, sorted by the median distance to telomeres for all genes in the genome. Only species with a median gene distance to the telomeres of above 15 Mb are shown, which is close to the maximal distance of established TPE-OLD genes from the telomere. Species proposed to age replicatively [as defined in Results and in (*18*)] are grouped on the left. The data presented in this figure serve as a reference for the preservation of telomeric distances below 20 Mb and for the differences between replicatively and nonreplicatively aging species that can be expected for TPE-OLD genes. We find the telomeric distances among established TPE-OLD genes to be preserved across species such that these appear as horizontal patterns on the left. The number in parentheses behind the gene name indicates the human chromosome coding for that gene. (**B**) Telomeric distances for TPE-OLD candidates among PP1A and PP2A subunits. This figure presents a selection of those genes that appear clustered below 20 Mb. The four genes that have been investigated here are marked in the legend.

cell growth, and response to stress were overrepresented in the group of TPE-OLD candidates (table S4). Thus, changes in the activity of these genes in aging cells may point to a regulated adaptive process, which prompted us to investigate one of the highly ranked groups of TPE-OLD candidates more closely.

Several regulatory subunit genes of the cell growth regulator PP2A are TPE-OLD candidates

Focusing on genes strongly related to cell growth and aging, 20 of the TPE-OLD candidate genes encode subunits of serine/threonine-specific phosphatases PPP1, PPP2, and PPP6 and display the typical positional conservation with respect to the telomere (Fig. 2B and figs. S2 to S3). These PPPs code for key regulators of cell division, protein synthesis, and tumor suppression. The most abundant enzyme, PP2A, accounts for up to 1% of total cell protein in some tissues and has more than 300 substrates involved in cell cycle and metabolism, regulating major cell cycle pathways and checkpoints (*16*, *17*). The full activity, substrate specificity, and subcellular localization of the PP2A phosphatase are determined by diverse regulatory subunits (Fig. 1B) (*16*, *17*). We observed that although the catalytic subunits (*PPP2CA* and *PPP2CB*) have high sequence conservation, their chromosomal positions were not conserved among species; in contrast, the telomeric distance of many regulatory subunit genes, which are much more diverse in sequence, tended to be evolutionarily conserved among species with TL-dependent replicative aging. In particular, we noticed that four regulatory subunits of PP2A, namely, *PPP2R2C*, *PPP2R2D*, *PPP2R5C*, and *PPP2R3B* (*21*–*24*), were locally preserved within the suggested TPE-OLD range at distinct positions relative to the telomere (fig. S4). No telomeric conservation (or any other conservation of chromosomal location) of these genes was observed in species that do not undergo TL-dependent replicative aging (Fig. 2B and fig. S4). Given these observations and the role of PP2A in cell cycle regulation, we focused on these four PP2A regulatory subunit genes as TPE-OLD candidates in our next experiments.

Expression of the PP2A regulatory subunit gene *PPP2R2C* is markedly up-regulated in healthy presenescent fibroblasts but is not up-regulated in stress-induced senescence

We examined telomere-associated changes in gene expression and cell physiology in old but still replicating (presenescent) cells. The presenescence stage (reached after high PDs) of primary cells was established by culturing cells until the final cell cycle arrest and, for the experiments, thawing frozen samples from 10 to 15 PDs before the suggested final arrest. The presenescent fibroblasts had already shortened telomeres [TL ratio (TLR) 0.15 to 0.24 versus TLR 0.48 to 0.81 in their young derivatives] but did not yet have the typical signs of senescent cells, even if their growth rate was already weakened (growth profiles are shown in fig. S5). These cells were compared with the respective replicatively young healthy cells. The same procedure was done with cells from patients with HGP, which are considered a model for accelerated telomere attrition and premature aging (*13*). TL was quantified as relative TLR, compared to single-copy gene standard, using an established polymerase chain reaction (PCR) method. Fibroblast cell lines were classified either as "young primary control cells" (low PDs 13 to 17, TLR 0.48 to 0.81), as "presenescent primary control cells" (high PDs 41 to 55, TLR 0.15 to 0.24), as "young primary HGP cells" (low PDs 19 to 20, TLR 0.28 to 0.68), or as "presenescent primary HGP cells" (high PDs 34 to 42, TLR 0.17 to 0.46; table S5).

First, we compared TL and gene expression levels of all relevant PP2A subunits in young (L for low PD in Fig. 3 and fig. S6) and presenescent (H for high PD in Fig. 3 and fig. S6) healthy controls and in HGP fibroblasts. Specifically, we analyzed the four PP2A regulatory subunits that appeared preserved within the suggested TPE-OLD range at distinct positions relative to the telomere (*PPP2R2C*, *PPP2R2D*, *PPP2R5C*, and *PPP2R3B*), the two structural (*PPP1A* and *PPP1B*), and the two catalytic subunits (*PPP2CA* and *PPP2CB*).

No influence of TL on gene expression was detected for any structural or catalytic subunit (Fig. 3). Among the regulatory telomeric PP2A subunit genes, *PPP2R2C* displayed a consistently up-regulated level of mRNA in healthy fibroblasts with short telomeres (6.85 ± 1.79-fold, $P \leq 0.01$ at 5 to 15 PDs before senescence),

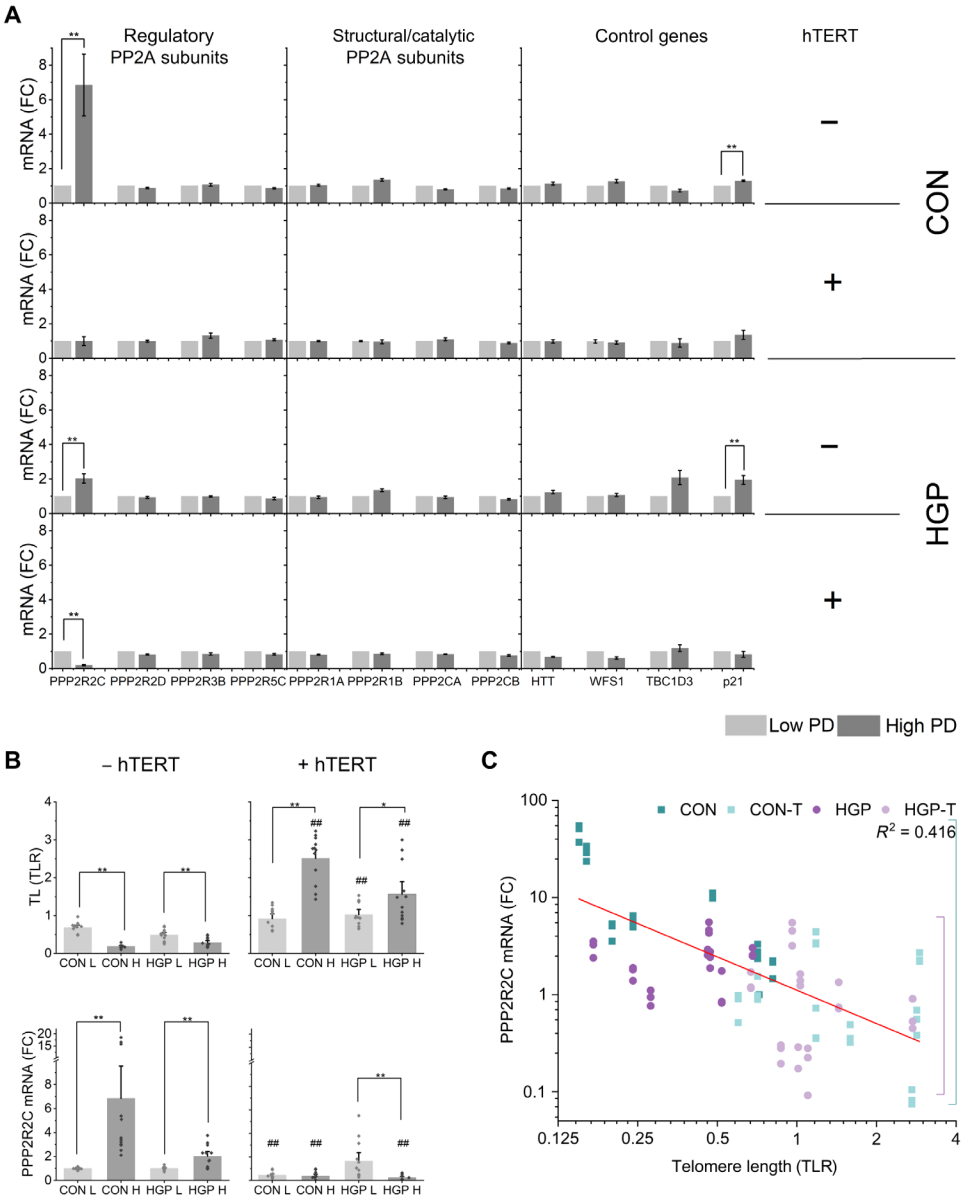

Fig. 3. TL-dependent mRNA levels of regulatory, structural, and catalytic PP2A subunits in control (CON) and progeria (HGP) fibroblasts. (**A**) Quantitative PCR (qPCR) analysis of primary (−hTERT) and immortalized (+hTERT) control (CON) and HGP cells at low (L) and high (H) PD. *Cyclophilin A* was used as normalization control. *WFS1* and *HTT* represent internal controls, *p21* represents a stress marker, and *TBC1D3* represents a potential confounder, as described in Results. All values were normalized to the level (=100%) of mRNA in cells at L PD. Results are shown as means ± SEM. Mann-Whitney *U* test was used: **P* < 0.05 and ***P* < 0.01 for L PD versus H PD. Six of 2394 measurements were excluded because mRNA was undetectable. (**B**) Average TL and *PPP2R2C* mRNA levels of CON and HGP cells at L and H PD before (−hTERT) and after (+hTERT) immortalization. TL was measured as relative TLR using monochrome multiplex qPCR (MMqPCR), as described in Materials and Methods. mRNA values were normalized to the level (=100%) of *PPP2R2C* mRNA in primary L PD cells. Results are shown as means ± SD. **P* < 0.05 and ***P* < 0.01 for L PD versus H PD. ##*P* < 0.01 for +hTERT versus −hTERT (Mann-Whitney U test). Each assay in (A) and (B) was performed in biological quadruplicate and technical triplicate. (**C**) Negative correlation between TL and *PPP2R2C* mRNA levels. All values were normalized to the mRNA level (=100%) of cell line 707 at L PD. Data are shown for 48 separate measurements from *n* = 16 cell lines [8 primary and 8 immortalized (T)], excluding one measurement with undetectable mRNA. FC, fold change.

with some interassay and interindividual variation (minimum/maximum observed fold change 2.76-fold/16.99-fold). The PP2A subunit genes *PPP2R2D*, *PPP2R5C*, and *PPP2R3B* were not up-regulated in fibroblasts under the conditions described here (Fig. 3A) and therefore were not analyzed further. In fibroblasts derived from patients with HGP, *PPP2R2C* mRNA levels increased 2.03 ± 0.27-fold, $P \leq 0.01$, in high PD cells relative to low PD cells (Fig. 3A) (minimum/maximun observed fold change 1.03-fold to 3.28-fold; fig. S6).

Next, we measured gene expression in h*TERT*-immortalized cells (i.e., cells with artificially elongated telomeres) at low and high PDs. Cells that had recently been immortalized were classified as "immortalized cells at low PD" (PD 14 to 28 after h*TERT* immortalization in healthy cells with TLR 0.6 to 1.18; PD 15 to 34 after h*TERT* immortalization in HGP cells with TLR 0.67 to 1.44), and cells with a substantial number of PDs after immortalization were classified as "immortalized cells at high PD" (PD 56 to 70 after h*TERT* immortalization in healthy cells with TLR 1.59 to 2.91; PD 57 to 63 after h*TERT* immortalization in HGP cells with TLR 0.87 to 2.74).

After immortalization, the *PPP2R2C* mRNA level in healthy fibroblasts was decreased to that of young cells or even lower (0.4 ± 0.3-fold versus 6.8 ± 6.2-fold, $P \leq 0.01$) (Fig. 3B). In HGP fibroblasts, the *PPP2R2C* mRNA level declined to below basal levels in h*TERT*-immortalized HGP fibroblasts (0.3 ± 0.2-fold versus 2.0 ± 0.9-fold, $P \leq 0.01$), but with a substantial delay (at high PD after immortalization only). Together, we found an inverse relationship between *PPP2R2C* expression and TL in both control and HGP fibroblasts (Fig. 3C).

In addition to replicative senescence, several factors can accelerate and/or trigger cell senescence, including various forms of stress like oxidative stress. Such acute stress is not primarily driven by the shortening of telomeres and may occur completely independently of TL and replicative senescence (*25*, *26*). Using sublethal H_2O_2 concentrations, we triggered stress-induced senescence to investigate the specificity of the phenomena described here. Cyclin-dependent kinase inhibitor p21 was used to monitor the stress-inducible premature senescence (SIPS) (*27*). We stimulated fibroblasts with H_2O_2 at concentrations capable of inducing a typical stress response (SIPS), as indicated by induction of *p21* mRNA (fig. S6) and the cellular stress marker β-galactosidase [i.e., senescence-associated β-galactosidase (SA-β-Gal)] (fig. S7). SA-β-Gal measurements were additionally confirmed by a highly sensitive spectrophotometric method [4-methylumbelliferyl-β-D-galactopyranoside (MUG)], an alternative for SA-β-Gal staining and subjective visual quantification that measures enzyme activity in cell lysates. We observed nonsignificant increases in *PPP2R2C* at the mRNA level in some experiments but found that H_2O_2 stimulation did not induce a significant *PPP2R2C* mRNA increase (fig. S6), while it did increase SA-β-Gal measurements, suggesting that oxidative stress is not a stimulus for *PPP2R2C* mRNA expression.

Together, these data showed that the expression of the PP2A regulatory subunit gene *PPP2R2C* is markedly up-regulated in healthy presenescent fibroblasts but is not up-regulated in SIPS. We found a lower relative increase in *PPP2R2C* mRNA in HGP cells compared to healthy controls but no marked deviation from the inverse relationship between TL and *PPP2R2C* expression.

Histone-dependent telomere looping but not long-range heterochromatin spreading is responsible for the silencing of *PPP2R2C*

We were next interested to explore the mechanism linking telomere shortening with *PPP2R2C* mRNA expression. Classical TPE in *Saccharomyces cerevisiae* and *Drosophila melanogaster* regulates genes in a manner proportional to the proximity to telomeric repeats through heterochromatin spreading and is not effective over longer telomere distances (*28*). To exclude spreading of the TPE in a continuous fashion (as in classical TPE), we examined the expression of other genes located between *PPP2R2C* and the telomere. We did not find a correlation between TL and the expression of genes such as *WFS1* and *HTT*, which also have some functional relationship with aging and survival (*29*, *30*), in high-PD and low-PD cells with and without hTERT immortalization (Fig. 3 and fig. S6). Thus, telomere attrition did not influence *WFS1* or *HTT* expression, although the chromosomal locations of these genes are more telomeric than the one of *PPP2R2C*, indicating that long-range heterochromatin spreading is not responsible for the silencing of *PPP2R2C*.

Next, we examined whether telomere shortening causes a change in chromatin organization involving the *PPP2R2C* locus. According to the TPE-OLD concept, there is a loop structure formed by long chromosomes in presenescent cells that opens or even completely disappears as telomeres shorten. Thus, as chromosomal reorganization occurs in cells with short telomeres, one would expect a higher percentage of separated ("S"; distance between probes >2.26 μm) probes and a lower percentage of adjacent ("A"; distance between probes <2.26 μm) probes. We used a high-resolution three-dimensional fluorescence in situ hybridization imaging (3D-FISH) to measure the distance between a bacterial artificial chromosome (BAC) probe containing the *PPP2R2C* locus (red; 4.2 Mb from the telomere) and a TelVysion probe containing the conserved subtelomeric region of 4p (green; ~100 to 300 kb from the telomere; Fig. 4). Consistent with our proposed mechanism, we observed a continuous and highly significant change in the overall distribution of the distances between the two loci in cells with long versus short TLs (Fig. 4 and figs. S8 and S9). This pattern persisted even when we examined the shortest and longest probe distances separately for each cell line (fig. S8D) to correct for the known bimodal distribution of TLs in fibroblasts (*31*).

In the yeast, expression of telomeric genes is modulated by chromatin modification in response to starvation and heat shock stress and is part of an important regulatory network (*28*). Moreover, changes in telomeric chromatin in late-passage human cells have been linked to cellular senescence (*32*). Heterochromatin in mammalian cells is normally dependent on histone deacetylation. We therefore investigated the influence of treatment with substances interfering with histone modifications on *PPP2R2C* mRNA levels (fig. S10). We did not find significant changes after treatment with trichostatin A (TSA), an inhibitor of histone deacetylases (*33*), and we did also not find a change after treatment of fibroblasts with 5-azacytidine (5-AzaC), which results in nonspecific overall DNA demethylation leading to a reorganization of genomic histone modification patterns (*34*). Resveratrol (RSV), which may induce instability of telomeric DNA (*35*), slightly increased *PPP2R2C* mRNA levels in h*TERT*-immortalized fibroblasts, by up to 1.6-fold.

Because TSA, 5-AzaC, and RSV lack specificity, we aimed for a more specific modulation. In *S. cerevisiae*, the nicotinamide adenine dinucleotide–dependent histone deacetylase Sir2 (silent information regulator 2) has a key role in generating and maintaining silent chromatin near telomeres (*36*). This epigenetic silencing of telomere-proximal genes is lost with replicative yeast aging, concomitant with aberrant hyperacetylation of subtelomeric sequences. The mammalian Sir2 homolog sirtuin 6 (SIRT6) has recently been shown to be required for repression of an endogenous telomere-proximal gene,

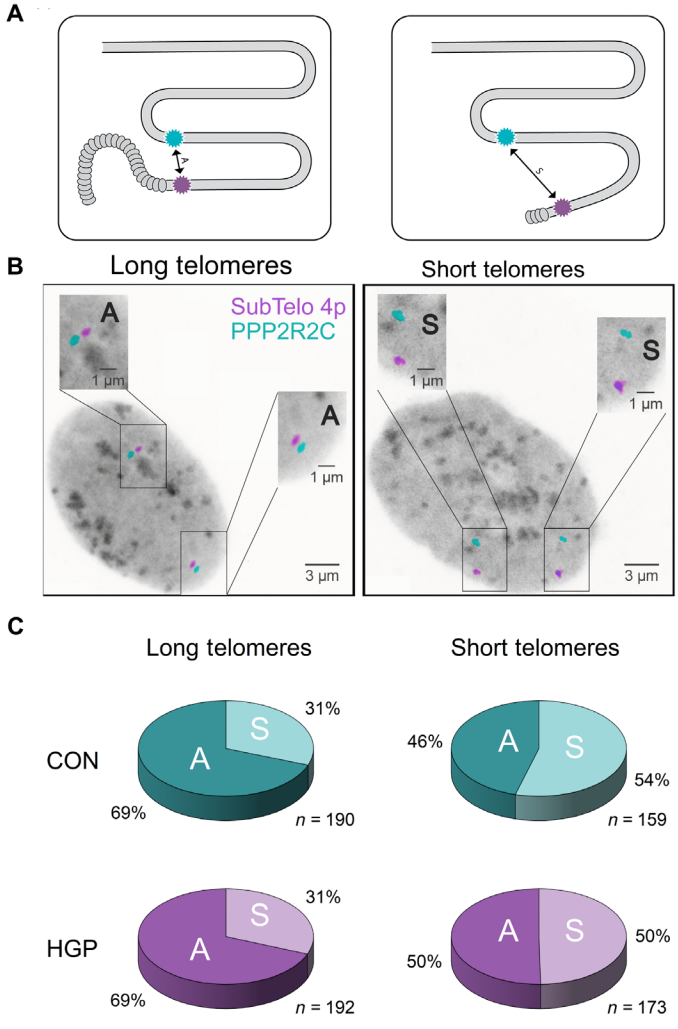

Fig. 4. Identification of *PPP2R2C* as a TPE-OLD gene: Chromosomal reorganization. (**A**) Graphical illustration of the TPE-OLD effect with long and short telomeres. (**B**) Confocal images of 3D-FISH processed with IMARIS. Gray, 4′,6-diamidino-2-phenylindole (DAPI); turquoise, BAC RP11-762B2 targeting the gene *PPP2R2C*; magenta, TelVysion (TEL) probe targeting subtelomeric 4p (100 to 300 kb from the telomere of chromosome 4p). A, adjacent; S, separated. (**C**) Overall distribution of TEL-*PPP2R2C* probe distances for both healthy control cells and progeria cells. The proportion of probe distances ≤2.26 and >2.26 μm is shown in circle diagrams. The number of experiments includes all data points, after deducting the points with fewer than or more than four signals (instead of two red and two green signals each), irregular DAPI staining (e.g., mitotic cells) and abnormal cell shape (252 of total 1680 distances were excluded). Images were acquired using 405-nm excitation/415- to 480-nm emission for DAPI, 488-nm excitation/500- to 545-nm emission for Spectrum Green, and 561-nm excitation/565- to 640-nm emission for Spectrum Orange. Images were then processed using Imaris 9.3 software (Andor Bitplane).

suggesting a key role for SIRT6 in maintaining a silencing-competent chromatin structure at natural telomeres (*37*). Compound BCI-150, a new SIRT inhibitor with selectivity for SIRT6 but not for SIRT1 and SIRT2 (*38*), enhanced the expression of *PPP2R2C* up to fivefold in h*TERT*-immortalized cells (fig. S10). As SIRT6 was found to be required for repression of telomere-proximal reporter genes in human cells (*37*), this finding suggests that silencing of *PPP2R2C* is dependent on histone deacetylation mediated by SIRT6.

P70S6K dephosphorylation and downstream effects in presenescent fibroblasts are directly related to *PPP2R2C* up-regulation regardless of basal mTOR levels

The protein encoded by *PPP2R2C* (PR55γ) inhibits p70S6K, a downstream target of mTOR, via dephosphorylation (*21*). Together with S6 ribosomal protein (S6RP) and initiation factor and 4E-binding protein 1, p70S6K is the most important downstream target of mTOR, and its Thr^{389} phosphorylation status closely correlates with its kinase activity in vivo (*39*).

In presenescent human fibroblasts, telomere attrition was associated with markedly decreased phosphorylation of p70S6K to 16 ± 6% of the levels of young healthy control cells (Fig. 5A). It has previously been shown that inhibition of p70S6K may secondarily decrease Akt phosphorylation (*40*). Accordingly, we observed a lower level of Akt protein in the phosphorylated state in both presenescent healthy controls and (to a lesser degree) HGP cells (Fig. 5C). Immortalization of cells with telomerase, which recovered cell growth (fig. S5), also recovered the p70S6K phosphorylation pattern (Fig. 5A) and the Akt phosphorylation pattern (Fig. 5C) in both cell types in a TL-dependent manner (fig. S11).

mTOR mediates and integrates growth signals; thus, mTOR and protein synthesis are tightly regulated and coupled to cell growth rates. We examined the possibility that a lower p70S6K degree of phosphorylation occurs secondary to a lower need for protein synthesis and a lower growth-related mTOR and p70S6K activity. We therefore related cell growth rates to the protein amounts of Akt, mTOR, and p70S6K (fig. S12). We found no evidence of a relationship between the growth rates, the expression of mTOR, p70S6K, and Akt, and the degree of p70S6K phosphorylation. By contrast, the HGP fibroblasts with reduced growth rates had approximately twofold higher relative mTOR, p70S6K, and Akt protein levels compared to control presenescent cells. Despite this inappropriately high mTOR activation, the deactivating dephosphorylation of p70S6K was not disturbed but was enhanced (red arrow in fig. S12). In another experiment, we examined the influence of serum starvation on total and phosphorylated p70S6K and mTOR protein and mRNA levels. As shown in fig. S13, this treatment led to slightly decreased levels of p70S6K and mTOR, reduction of which, however, was much lower than the TL-dependent up-regulation of *PPP2R2C* and the resulting decrease in p70S6K phosphorylation in aged cells. Thus, serum starvation was not a major determinant of p70S6K phosphorylation in presenescent fibroblasts.

Phosphorylation at Thr^{389} activates p70S6K and increases cellular protein synthesis via phosphorylation of the S6RP; correspondingly, dephosphorylation inhibits protein synthesis. Inhibition of mTOR (and p70S6K) decreases the protein levels of many metabolic targets and may thus decelerate senescence entry. We therefore analyzed the metabolic marker arylsulfatase A (ARSA), in primary presenescent cells. The protein product (fig. S14, right) and resulting activity (middle panel) of ARSA, which is regulated by mTOR and p70S6K and is strongly inhibited by the prototype mTOR inhibitor rapamycin (*41*), were suppressed in aged fibroblasts.

To further confirm the role of *PPP2R2C* in p70S6K phosphorylation in fibroblasts, we performed inhibitor experiments using *PPP2R2C*-specific small interfering RNA (siRNA). Upon treatment of presenescent fibroblasts with siRNA (both 25 and 50 nM) for 7 hours and an incubation time of 48 hours after siRNA removal, the dephosphorylation of p70S6K was inhibited by approximately 90% in HGP cells (fig. S15). In parallel, increased mRNA levels of

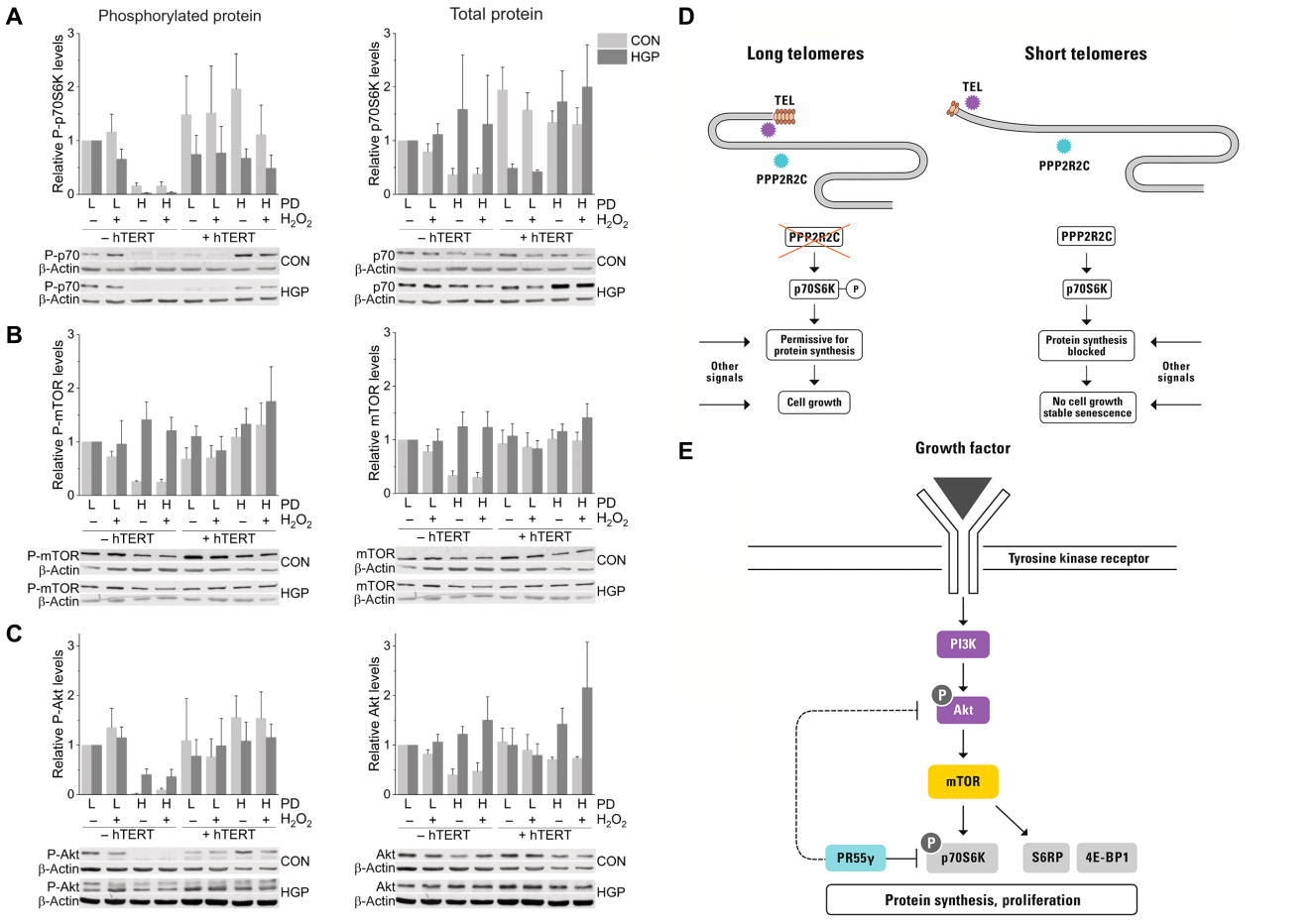

Fig. 5. Influence of TL on mTOR signaling. (**A** to **C**) Total and phosphorylated protein levels of (A) p70S6K, (B) mTOR, and (C) Akt. Western blot analysis was performed from primary (–h*TERT*) and h*TERT*-immortalized cells (+h*TERT*) at low (L) and high (H) PDs in the absence or presence of H_2O_2 (200 μM; 2 hours), as indicated. Light gray columns, healthy CON fibroblasts; dark gray columns, HGP fibroblasts. All protein levels were normalized to the protein levels of β-actin. Protein/β-actin ratios were expressed relative to those in low-PD cell samples (which were set at a value of 1). Means ± SEM, $n = 4$ cell lines per column (with two to three independent blots each). Each β-actin belongs to the same membrane as the respective protein (fig. S21). (**D**) Schematic summary of the suggested protective effect of TPE-OLD on *PPP2R2C* (PR55γ for the protein) induction. (**E**) Schematic illustration of the Akt/mTOR/p70S6K pathway. PR55γ-mediated dephosphorylation of p70S6K has a direct inhibitory effect on protein synthesis and may thus stabilize cells in presenescence. Inhibition of p70S6K may additionally lead to a lower degree of Akt phosphorylation (*40*). Magenta, oncogenes; turquoise, tumor suppressors; gray, not characterized. PI3K, phosphatidylinositol 3-kinase; 4E-BP1, 4E-binding protein 1.

genes whose transcription is likely dependent on p70S6K phosphorylation were observed and the total amount of p70S6K was moderately reduced. Together, these findings are in accordance with previous data on p70S6K and show that TL-dependent up-regulation of *PPP2R2C* leads to metabolic and proliferative suppression in aged cells. Our data support the notion that PR55γ, which is encoded by *PPP2R2C*, causes dephosphorylation of p70S6K and thereby contributes to inhibition of cellular function in presenescent fibroblasts with short telomeres.

TL-dependent silencing of *PPP2R2C* and possible downstream effects were not severely affected in HGP fibroblasts despite abnormalities in telomere attrition kinetics

Fibroblasts from patients with HGP were used as a model for suggested accelerated telomere attrition. The mean TL in HGP fibroblasts is slightly shorter than normal, and the TL distribution is abnormal. Normal or even longer telomeres have been described in approximately one-third of all cells (*13*, *14*). We therefore hypothesized that changes in TPEs may at least in part explain these aging-related phenomena. However, we could exclude a severe abnormality in TPE-OLD (for *PPP2R2C*) in HGP.

p70S6K was almost completely unphosphorylated in presenescent HGP cells (Fig. 5A); we observed an inverse relationship between TL and *PPP2R2C* mRNA expression (Fig. 3C), and dephosphorylation of p70S6K occurred in aged HGP cells with shorter telomeres (Fig. 5A) despite constantly high levels of total mTOR protein levels in these cells (fig. S12), which together excludes a severe abnormality in TL-dependent silencing of *PPP2R2C* by TPE-OLD.

There were, however, various indications of some subtle "telomeric dysfunction" in HGP cells. For example, in cells from patients with HGP but not controls, telomeres tended to be shorter in young cells (TLR 0.49 ± 0.08 in HGP versus 0.68 ± 0.07 in controls at low PD; $P = 0.1$) but longer in presenescent cells (TLR 0.33 ± 0.08 versus

0.19 ± 0.02 at high PD; $P = 0.2$) (Fig. 3B). TL-dependent chromosomal reorganization in HGP fibroblasts was slightly (~10%) but not significantly different from that in controls (table S6). In line with the abnormal TL distribution, there was a higher variability in other features examined in HGP cell lines. Two HGP cell lines (HGADFN 127 and HGADFN 164) showed only moderate chromosomal reorganization, whereas the third cell line (HGADFN 178) displayed the most severe reorganization among all cells (fig. S9). Moreover, we found a lower relative increase in *PPP2R2C* mRNA in HGP cells compared to healthy controls (2.03 ± 0.27 versus 6.85 ± 1.79-fold, $P = 0.02$; Fig. 3B), and the suppression of Akt phosphorylation was reduced in HGP cells compared to the controls (41 ± 11% versus 2 ± 1% of phosphorylation levels in young cells, $P = 0.029$; Fig. 5C). We also observed higher overall proliferation rates (figs. S5 and S16) and an approximately 2-fold higher activity level of the mTOR target ARSA ($P = 0.04$) and an approximately 1.5-fold higher ARSA protein level compared to control cells (difference not significant) (fig. S14), associated with a higher degree of senescence. Primary HGP cells grew faster and senesced after fewer rounds of replication than healthy control cells (fig. S5). We observed a higher fraction of cells in the G_2-M phase of the cell cycle (fig. S14) typical for senescent cells (*42*), higher levels of the senescence markers MUG and SA-β-Gal (fig. S7), elevated levels of mTOR in presenescence, and elevated levels of *TBC1D3* (Fig. 3 and fig. S6), an amplifier of EGF receptor response. Together, these findings indicate that HGP cells have higher proliferation stress than controls. Although a severe abnormality in TPE-OLD (for *PPP2R2C*) can be excluded, TL heterogeneity and/or dysfunction may lead to altered TPE-OLD dynamics that may contribute to a higher degree of proliferation stress.

TL-dependent silencing of *PPP2R2C* and established TPE-OLD candidates in other cell types and in fibroblasts from aged cell donors

To investigate TL-dependent expression of *PPP2R2C* in a different human cell type, we assessed the expression of *PPP2R2C* and TLs in 413 lymphoblastoid cell lines (LCLs) established from B lymphocytes from participants of the Berlin Aging Study II (BASE-II) (*43*, *44*), using the reverse transcription PCR (RT-PCR) and monochrome multiplex quantitative PCR (MMqPCR) approaches used for fibroblasts above. LCLs are expected to represent cells with a very broad TL distribution. Using this cell population, we did not observe a correlation between *PPP2R2C* expression and TL (fig. S17). We did also not find an increased mRNA expression for the other TPE-OLD candidates in LCLs. In primary human umbilical vein endothelial cells (HUVECs), by contrast, we found mRNA up-regulations for *PPP2R2C*, *PPP2R2D*, *PPP2R5C*, *C1S*, and *SORBS2*; we found a reciprocal regulation (lower mRNA levels in aged cells) for *DSP* and no significant changes or inconclusive results for *TERT*, *ISG15*, and *PPP2R3B* (fig. S18). In human fibroblasts, we could confirm most of the previously established TPE-OLD genes as being differentially expressed (higher expression in aged cells with short telomeres), but we could not show differential regulation for *PPP2R5C*, *PPP2R2D*, and *PPP2R3B*. Together, these data suggest that cell specificity is to be noted for TPE-OLD and/or that other factors may influence the expression of these TPE-OLD genes, particularly in LCLs (fig. S18).

We lastly asked whether up-regulation of *PPP2R2C* also plays a role in vivo and thus compared fibroblasts derived from very young up to very old individuals. We found that up-regulation of *PPP2R2C* is evidently more pronounced in the cells from very old donors, compared to young and middle-aged cell donors, further suggesting a physiological function in the aging organism and that in vitro replicative senescence resembles in vitro senescence (fig. S19).

DISCUSSION

A simple tool predicts known and candidate TPE-OLD genes

We presented a heuristic strategy that can be applied to identify potentially protective TPE-OLD candidate genes. Most of these candidate genes are not known to be involved in senescence or apoptosis entry but code for proteins involved in proliferation, metabolism, tumor suppression, and stress response. Moreover, many TPE-OLD candidates are regulated by transcription factors involved in proliferation, development, and stress response. For example, the functions of the AP2 family of transcription factors are the cell type–specific stimulation of proliferation and the suppression of terminal differentiation (*45*). Sp1 both activates and suppresses the expression of a number of essential oncogenes and tumor suppressors, as well as genes involved in proliferation, differentiation, DNA damage response, and senescence (*46*).

Only 1 of the 11 human genes associated with the Gene Ontology (GO) term "chromatin silencing at telomere" (GO:0006348) was found within the group of TPE-OLD candidate genes, *DOT1L*, which encodes a histone H3K79 methyltransferase and is essential for mammalian heterochromatin structure. Hence, the group of 2322 genes described here likely belongs to a previously unknown category with regulation being dependent on TL. Our tool allows other researchers to identify and investigate possible TPE-OLD genes for unidentified antitumor and antiaging strategies.

The gene encoding for the protein phosphatase 2A subunit PR55γ (*PPP2R2C*) is a TPE-OLD gene and subject to long-range telomere regulation in human fibroblasts

PPP2R2C up-regulation was dependent on telomere attrition but not on exogenous stress triggers such as H_2O_2. Complete gene silencing was achieved by telomere elongation. Using 3D-FISH analysis, we showed that TEL-*PPP2R2C* probes were significantly closer together in cells with long telomeres than in cells with short telomeres, demonstrating telomere-dependent chromatin reorganization. In accordance with other investigations, changes in TPE-OLD gene expression were discontinuous (e.g., not involving genes positioned closer to the telomere), and the reestablishment of gene suppression after h*TERT* introduction occurred with some delay (as some time is required for elongation) (*47*).

Notably, BCI-150, a recently developed SIRT inhibitor with selectivity for SIRT6 versus SIRT1 and SIRT2 (*38*), enhanced the expression of *PPP2R2C* up to fivefold in h*TERT*-immortalized cells. As SIRT6 is required for repression of telomere-proximal reporter genes in human cells (*37*), this finding suggests that silencing of *PPP2R2C* is dependent on histone deacetylation mediated by SIRT6. The bimodality in 3D-FISH experiments suggested that both chromosomes are involved in telomere loopings, in accordance with the reported bimodal distribution of TLs in fibroblasts, with TL differences of up to 6.5 kb between homologous chromosomes, likely due to stochastic elements in telomere inheritance (*31*). Together, these findings demonstrated a mechanistic link between TPE-OLD and a tumor suppressor gene that acts long before telomere-driven DNA damage signaling occurs.

Telomere attrition leads to suppression of mTOR signaling via dephosphorylation of p70S6K

It has previously been shown that overexpression of *PPP2R2C* inhibited cancer cell proliferation both in vitro and in vivo through the suppression of the activity of S6K in the mTOR pathway (*21*). Vice versa, low *PPP2R2C* expression was associated with an increased likelihood of cancer recurrence and cancer-specific mortality in prostate cancer (*48*). In accordance with these data, we showed that *PPP2R2C* up-regulation led to almost complete dephosphorylation of p70S6K in presenescent but still replicating fibroblasts, and we found inverse relationships between TL and *PPP2R2C* expression and between TL and the dephosphorylation grade of p70S6K and Akt, respectively. Dephosphorylation of p70S6K likely delays senescence entry via metabolic suppression. The protein synthesis of rapamycin-sensitive proteins was suppressed in presenescent fibroblasts. By contrast, inhibition of *PPP2R2C* by siRNA may reinduce mTOR/p70S6K-dependent genes in aged cells. In parallel, we observed a decline in total p70S6K protein, which may occur because of phosphorylation-dependent degradation events, as previously described (*49*). However, we cannot entirely exclude unspecific transfection events (*50*). More specific and complete knockout and overexpression strategies using CRISPR-Cas9 technologies may further elucidate possible beneficial effects of *PPP2R2C*.

The combination of expansion-stimulation signals and inhibition of cell division (*51*) is a well-known factor in the transition to an unstable hypermetabolic state, which may occur without effective down-regulation of cell metabolism (*52*). Our data corroborate other findings and suggest an overall protective effect of p70S6K dephosphorylation in presenescent cells. This molecular pathway and the life-prolonging effects of mTOR suppression have been discussed in great detail. However, most findings so far were obtained by use of genetic manipulation in mice (*53*, *54*) and flies (*55*) or mTOR inhibition in human and rodent cell lines or in *Caenorhabditis elegans*. We show a possible physiological function and mechanism for mTOR suppression in vivo and identify short telomeres as an upstream trigger for mTOR suppression.

The effects of *PPP2R2C* regulation by TL supports the hypothesis that replicative aging fulfills a tumor suppressor function in vivo

The here-described findings strongly argue for a tumor suppressor function of replicative aging. We identified a direct tumor suppressor gene under influence of TPE-OLD. A protective effect that mitigates the pitfalls of telomere attrition, namely, ongoing mitogenic stress, is plausible and supports the hypothesis that a main function of replicative aging is tumor suppression. As a prerequisite for an overall positive net effect (tumor suppression for a sufficiently long period of time), possible negative aspects of replicative aging must be minimized. Telomere attrition is, genetic instability syndromes (*56*) notwithstanding, generally not life-threatening in humans and also not in mice nor in *C. elegans* (*57*–*59*).

The expression of the *hTERT* gene itself is possibly regulated by TPE-OLD (*12*), further pointing to a regulatory role of telomeric gene expression. Gene silencing may have evolved as a mechanism to suppress undesired gene expression after embryonal development. It is tempting to speculate, but awaits further experimental proof, that limited up-regulation of *hTERT* in a cell with critically short telomeres may stabilize the cell without undermining the tumor suppressor effect of telomere attrition in general; "mild" *hTERT* up-regulation and mTOR suppression may synergize to limit the tumorigenic risk in cells with critically short telomeres. These data do not exclude the possibility that the induction of h*TERT* or other TPE-OLD genes may paradoxically impinge on the predisposition to cancer through uncontrolled transcriptional derepression.

HGP fibroblasts display functional *PPP2R2C* TPE-OLD effects but abnormalities in telomere attrition kinetics

Our experimental data did not indicate severe deficiency of TL-dependent chromosomal reorganization in HGP. Thus, functional chromosomal reorganization may prevent an even worse phenotype, which is in line with the low cancer rates among patients with HGP (*15*).

Despite functional TPE-OLD in HGP fibroblasts, HGP cell lines display some abnormalities such as reduced mean *PPP2R2C* mRNA levels, higher proliferation rates, a reduced degree of Akt suppression, elevated variability of TL in 3D-FISH experiments, less marked changes in telomere *PPP2R2C* probe distances between low- and high-PD cells, and a slightly lower suppression of the metabolic marker ARSA. These observations are plausible in view of the greater heterogeneity in TL and abnormal TL distribution in HGP found in this and other studies; normal or even longer telomeres have been described in approximately one-third of all cells in other studies despite shorter average TLs (*13*, *14*). Accordingly, we detected shorter telomeres in young HGP cells and even longer telomeres in presenescent cells, which corresponds to an overall "narrower" and shifted TL and *PPP2R2C* expression range. Primary (but not h*TERT*-transfected) HGP cells grew faster and senesced earlier after fewer rounds of replication (figs. S5 and S16). Altered dynamics in gene activation/silencing may contribute to attenuated metabolic suppression, which is known to accelerate senescence entry (*52*).

HGP fibroblasts age much faster in vitro and show constitutive activation of mTOR signaling, whereas the dephosporylation of p70S6K is apparently intact. Preliminary data suggest more pronounced alterations in other TPE-OLD genes. Together, these data point to telomeric abnormalities in HGP and may help to explain why patients with HGP do not develop tumors but many signs of premature aging. Because of the early death of patients with HGP, it cannot entirely be ruled out that an increased risk of cancer could arise with older age in these patients. To investigate telomere clinical phenotype interrelationships more closely, cells from patients with Nijmegen breakage syndrome (*56*), which is characterized by chromosome instability, could be helpful. In fibroblasts from these patients, there were also indications of telomeric imbalances in TPE-OLD associated with accelerated telomere attrition (*56*). The patients tend to have progeroid symptoms, but, in contrast to patients with HGP, they have shorter telomeres, a higher degree of genetic instability, and a high cancer rate.

The TPE-OLD mechanism is evolutionary conserved, likely as a response to negative effects of replicative aging

Several lines of evidence support our hypothesis that TPE-OLD is an evolutionarily conserved response to replicative aging. First, we did not find an equal distribution of TPE-OLD genes along the ends of the chromosomes, indicating a highly conserved telomeric localization. Second, TPE-OLD candidates have functional similarities and are often involved in the control of proliferation and metabolism or stress responses. We anticipate that many other genes beyond the known ones such as *PPP2R2C* are protectively activated by

TPE-OLD as the cells of humans and other large, long-lived species age. We observed telomeric clustering of many other genes related to stress and aging, including interleukins (fig. S20), tumor suppressor genes, and genes coding for *FOX* (forkhead box) transcription factors involved in insulin signaling and longevity and heat shock factor 1 (*HSF1*), the master regulator of proteotoxic stress, but we did not find such clusters for genes involved in development, such as *HOX* genes or for the cell death gene and canonical driver of inflammation nuclear factor NF κB, which is in agreement with our concept that TPE-OLD is effective in presenescent cells and triggers protective processes but does not trigger apoptosis. Third, there are obvious similarities to classical TPE. The main function of classical TPE is protection against acute cellular stress. Notably, *CDC55*, the ortholog of *PPP2R2C* in yeast, is located in relative proximity to the yeast telomere (<150,000 base pairs), a site at which classical TPE with heterochromatin spreading and silencing of adjacent genes can be effective. CDC55 encodes YGL190C, which dephosphorylates and antagonizes the protein Tap42, mediating the effects of rapamycin on the yeast Tor protein kinase (*60*). CDC55 stabilizes yeast cells during starvation-induced stress and down-regulates metabolic functions (*61*). This mechanism is strongly reminiscent of the metabolic effect of p70S6K inhibition in humans. We thus suggest that TPE in yeast and TPE-OLD in large, long-lived species have a common functional and mechanistic origin (Fig. 6).

TPE-OLD effects are cell type specific and/or may display further levels of regulation

A differential regulation of *PPP2R2C* mRNA could be demonstrated for HUVECs and fibroblasts but not for LCLs. Moreover, a differential regulation of most known TPE-OLD genes could be shown for HUVECs and fibroblasts but not for LCLs suggesting cell specificity and/or peculiarities in LCLs.

Considering cell type specificity, the three other PP2A subunit TPE-OLD candidates affect similar pathways, and all potentially attenuate cell proliferation via mTOR inhibition (Fig. 1B), raising the possibility that these subunits may be induced in other metabolic states or in other cell types. Findings from facioscapulohumeral muscular dystrophy, in which a genetic defect results in repositioning of an active gene near telomeres or subtelomeric sequences and the phenotype is altered in an age-dependent manner (*9*), suggest cell and tissue specificity for TPE-OLD. TL varies greatly across tissue types (*62*); hence, similar functions may be performed by different subunits with genomic positions appropriate for the basal TL of their respective cell types.

There are various other possible explanations for discrepant findings in different cell types. It is possible that splice variants are induced, some of which undetectable with the used universal primer pairs. In addition, epigenetic mechanisms may influence TPE-OLD effects including DNA methylation and histone modifications in promotor regions (*12*), which are difficult to control experimentally. For example, in Epstein-Barr virus–transformed lymphoblastoid cells, the immortalization procedure may have contributed to the inability to reproduce established TPE-OLD effects. In these cells, telomeres are elongated both by telomerase and by alternative lengthening of telomeres, which may result in dysfunctional telomeres with a reduction in telomere binding proteins (*63*). We were interested that the in vitro effects of *PPP2R2C* were most pronounced in cells from three very old donors, further suggesting a physiological function of TPE-OLD (*PPP2R2C*) in the aging organism.

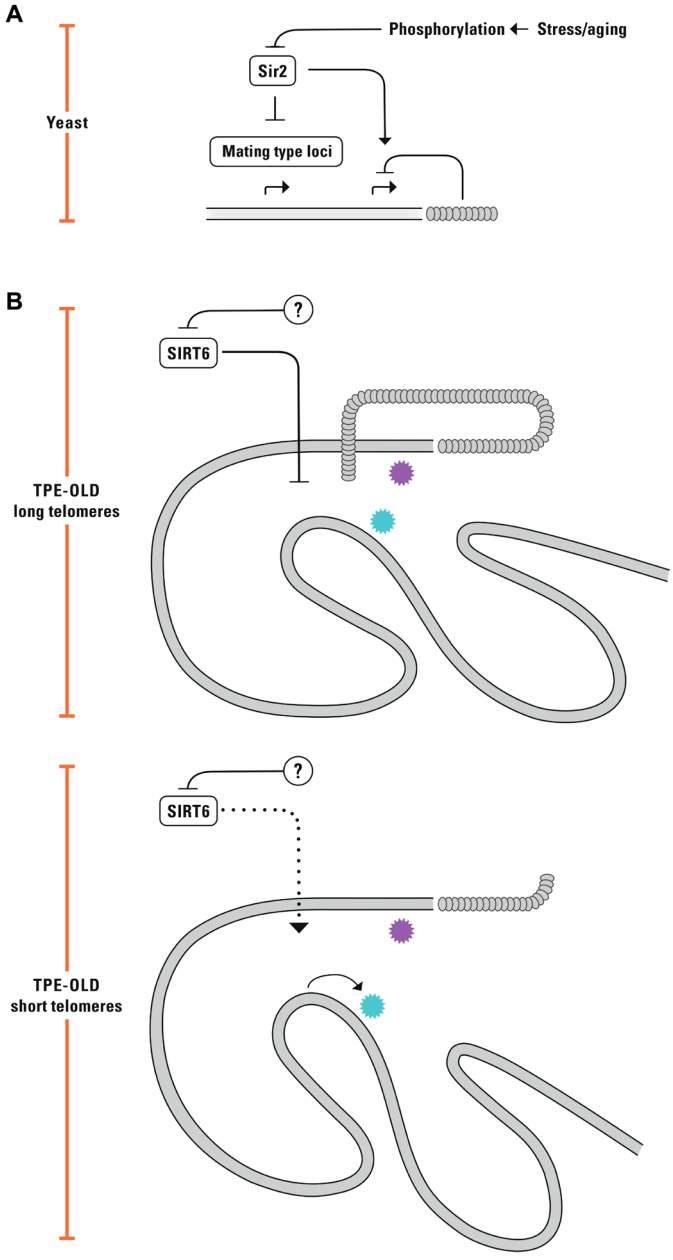

Fig. 6. Similarities between TPE and TPE-OLD and possible phylogenetic relationships. (**A**) TPE-OLD and TPE in yeast may share mechanistic and functional aspects. In *S. cerevisiae*, under optimal growth conditions, most subtelomeric genes are silenced by the histone-binding silent information regulator (SIR) complex (in this species, largely independent of TL). Nutrition starvation, heat shock, or chemical treatment can induce hyperphosphorylation of Sir proteins and a subsequent decrease in silencing (*28*). (**B**) Mechanistic and functional similarities of TPE in yeast and TPE-OLD in mammals and other vertebrates may be due to common evolutionary heritage, with SIRT6 (the mammalian homolog of Sir2) retaining its ancestral role as a cofactor for gene silencing in young and growing cells in the same way as Sir2 acts as a silencing factor in yeast, with stress serving as its inhibitor via phosphorylation events.

Cell specificity together with redundancy and methodological challenges (e.g., the difficulty in detecting these subtle effects without artificial cell manipulation) may explain why TPEs have thus far not been reported for human cells on a larger scale. Other tissues and other PP2A regulatory subunits and other TPE-OLD candidates

must be examined to unravel cell specific effects. More structural experiments are required for a better understanding of how chromatin architecture may influence TPE-OLD. These experiments include combining chromatin interaction maps with epigenome and transcriptome datasets for studying long-range control of gene expression. Another limitation of the here-described approach are possible misassignments to the classes of replicatively and nonreplicatively aging species, respectively. For example, there is little data on the cetaceans, and it seems possible that the blue whale, the narwhal, and the vaquita also age replicatively. For each new TPE-OLD candidate, confirmatory studies should be performed to confirm TPE-OLD effects experimentally and to rule out piggybacking by gene synteny as a cause for the telomeric location, e.g., the physical colocalization of genetic loci that are not disrupted during evolution.

In conclusion, we have identified a physiological trigger (telomere attrition) for a well-known aging-protection mechanism (mTOR suppression). This mechanistic link between short telomeres and tumor suppression points to a tumor suppressor function of replicative aging. We identified a large number of new TPE-OLD candidate genes, and we present a heuristic strategy that can be applied to easily identify candidate TPE-OLD genes. TPE-OLD genes are potential targets for intervention in cancer- and aging-related processes. Their activation may have a protective effect when telomeres shorten, but they do not necessarily have beneficial effects under all circumstances, such as in disease-associated cellular states.

MATERIALS AND METHODS

Experimental design

Genes with potential for TPE-OLD were screened in silico with cross-species data from the Ensembl genome database. We focused on a group of genes that shows preserved telomeric distances and that is strongly related to cell growth and aging.

The aim of further investigations was to examine telomere-associated changes in gene expression and cell physiology in old but still replicating (presenescent) cells before the point of cell cycle arrest. The presenescence stage (high PDs of primary cells) was established by culturing cells until the final cell cycle arrest and thawing frozen samples from 10 to 15 PDs before the final arrest for experiments.

Retrieval of gene-telomere distances for human genes and their orthologs

We retrieved the gene-telomere distances from the public MySQL database of Ensembl Mart version 100 (released April 2020) (*64*). Orthologs were accepted as determined by Ensembl Compara (*65*) by the "one2one, "one2many," or "many2many," definitions. A species was included into the analysis if it was one of the established model organisms (*S. cerevisiae* and *C. elegans*) or if its median gene-telomere distance was at least 7.5 Mb, i.e., the median distance for fruitfly, as a threshold for the quality of genome assemblies in Ensembl to avoid false positives at the ends of chromosomal fragments. To facilitate interpretation, species are indicated by their common name. Scatter plots were created with R (*66*) version 4.0.1 and the ggplot2 package; heatmaps were created with the gplots (*67*) package for custom selection of genes from gene families with known gene-position effects. Telomeres are not annotated in Ensembl. As the biological anchor to define the gene-telomere distance for our analysis, we chose the location of the gene on the same chromosome arm that is closest to the telomere, i.e., the first (p arm) or last (q arm) coding sequence for each chromosome.

Determination of preserved telomeric distances and selection of TPE-OLD candidates

For each gene, we determined at which distance to the telomeres the largest number of orthologs are located, where the maximum allowed pairwise distance between chromosomal positions was set to 1 Mb. We allow for two such 1-Mb-wide regions for each gene. The sum of the number of orthologs covered in these two regions determines the rank of that gene as a TPE-OLD candidate. For Fig. 1B and figs. S1 to S3, we thus grouped the chromosomal positions of the orthologs using a parameter-free complete linkage tree, using the R function hclust, for which we provided a custom distance function and then used the routine "cutree." We systematically iterated over all human genes in Ensembl 104 with at least 12 orthologs in all completely sequenced "replicatively aging" species.

In the scatter diagrams of Fig. 2, the species on the x axis are sorted primarily by replicatively aging versus "nonreplicatively aging" and secondarily by their median gene-telomere distance. Scatter plots represent genes by a unique symbol and show telomeric distance on the y axis. Positions above 20 Mb are clipped in the scatter plot.

All R and shell scripts contributing to this manuscript are available online (*68*) to facilitate updates with upcoming releases of Ensembl or custom gene selections. The criteria for categorizing a species as having assumed TL-dependent replicative aging (marked by green color) were set as TL < 20 kb, undetectable telomerase levels, and no stasis, as described previously (*18*).

Gene set enrichment analysis

Gene enrichment analysis was performed by g:profiler as described in (*19*). Briefly, an enrichment score (ES) is calculated that reflects the degree to which a set S is overrepresented at the extremes (top or bottom) of the entire ranked list L. The statistical significance (nominal P value) of the ES is estimated by using an empirical phenotype–based permutation test procedure that preserves the complex correlation structure of the gene expression data. The proportion of false positives is controlled by calculating the false discovery rate by comparing the tails of the observed and null distributions for the normalized ES.

Cells and cell culture lines

Human primary dermal fibroblast cell lines were obtained from The Progeria Research Foundation (PRF) Cell and Tissue Bank. The HGP cell lines were HGADFN003, HGADFN127, HGADFN164, and HGADFN178. All HGP cell lines displayed the classical HGP mutation [LMNA Exon 11, heterozygous c.1824C > T (p.Gly608Gly)] [more details in (*69*)]. We did not examine cell lines with nonclassical or multiple mutations (exclusion criterion). Histograms of mutational analysis sequenced by the PRF Cell and Tissue Bank are available on request. Healthy child control dermal fibroblast cell lines (707, 731, 778, and 811) were a gift from the Children's Hospital of Münster (Professor Thorsten Marquardt). These fibroblasts were from children in whom a genetic disease has been excluded and a nongenetic cause for their symptoms had been found. Cultures from all cell lines have tested negative for mycoplasma contamination. Ethical approval for the establishment of the cell lines and informed consent were obtained from the children's parents. One human primary

dermal fibroblast cell line from an adult donor (N14) was a gift from E. Orso, University of Regensburg. The characteristics of all fibroblast cell lines are summarized in table S5.

All human fibroblasts were maintained in Dulbecco's modified Eagle's medium (DMEM) high glucose (4.5 g/liter) with L-glutamine without pyruvate (Gibco, catalog no. 41965) supplemented with 10% fetal bovine serum (FBS; Biochrome), penicillin (100 U/ml), and streptomycin (100 μg/ml) (Biochrome, catalog no. A2212), hereafter referred to as "fibroblast medium." In addition, we analyzed mRNA from healthy human fibroblast donors at different ages.

The 1301 cell line (derived from T lymphoblastic leukemia) was a gift from S. Roura (ICREC Research Group, Institut d'Investigació en Ciències de la Salut Germans Trias i Pujol, Barcelona, Spain). All other LCLs were established from BASE-II participants. We analyzed a subgroup of 413 participants of the BASE-II selected on the basis of the availability of LCLs. BASE-II is a prospective multidisciplinary and multi-institutional study that investigates factors associated with aging trajectories in Berlin (*43*, *70*). All participants gave written informed consent to the study protocol that was approved by the Ethics Committee of the Charité-Universitätsmedizin Berlin (number of the ethical approval: EA2/ 029/09). Both the 1301 cell line and LCLs from the BASE-II study were maintained in RPMI 1640 medium with L-glutamine (Gibco, catalog no. 11875-093) supplemented with 10% FBS (Biochrome), penicillin (100 U/ml), and streptomycin (100 μg/ml) (Biochrome, catalog no. A2212). All cells were grown at 37°C in a humidified incubator containing 5% CO_2.

HUVECs were obtained from PromoCell (catalog no. C-12200; LOT no.: 449Z004) and cultivated using the Endothelial Cell Growth Medium Kit (catalog no. C-22110) from the same company. Penicillin (100 U/ml) and streptomycin (100 μg/ml) from Thermo Fisher Scientific (catalog no. 15140122) were added to the medium. HUVECs at several passages were grown in a humidified incubator at 37°C and 5% CO_2. Expansion, cell cultivation, and experiments were performed in T75 cell culture flasks (Sarstedt, catalog no. 83.3911.302). High cell densities were selected for subsequent harvesting.

h*TERT* immortalization

Fibroblasts were infected with retroviral supernatants from a packaging cell line (PA317-TERT) that stably expresses human telomerase cloned into a pBabePuro vector according to methods previously described (*47*, *71*). The vector and packaging cell line were a gift from W. Wright (UTSW Medical School, Dallas, TX, USA). After a 2-week selection with puromycin according to established protocols (*47*), infection and selection were checked by determination of h*TERT* expression using real-time PCR and measurement of TL as described (*72*).

Test points for measurements

Test points for the fibroblast cell lines were classified either as "primary cells at low population doubling (PD)" (PD 13 to 20) or as "primary cells at high PD" (PD 34 to 55). The presenescence stage (high PDs of primary cells) was established by culturing cells until the final cell cycle arrest and thawing frozen samples from 10 to 15 PDs before the final arrest for experiments. Cells that had recently been immortalized were classified as immortalized cells at low PD (PD 14 to 34 after h*TERT* immortalization), and cells with a substantial number of PDs after immortalization were classified as immortalized cells at high PD (PD 55 to 70 after h*TERT* immortalization). The fibroblasts were immortalized in medium PDs, at about the same time interval before senescence (mean PD of immortalization in controls PD 37 and in HGP PD 20).

Hydrogen peroxide treatment

Cells from eight fibroblast cell lines (HGADFN003, HGADFN127, HGADFN164, HGADFN178, 707, 731, 778, and 881) were grown to 100% confluence in 10-cm dishes. For H_2O_2 treatment, two culture dishes of each cell line were treated for 2 hours with 200 μM H_2O_2 in 10 ml of fibroblast medium; an additional three dishes were processed identically but without H_2O_2. After 2 hours of incubation, the cells were washed with 5 ml of PBS (Gibco, catalog no. 14190250) and incubated in fresh fibroblast medium for another 22 hours. Subsequently, cells from one H_2O_2 dish and from one untreated dish (as a control) for each of the eight cell lines were harvested for Western blot analyses. In addition, cells from the H_2O_2-stressed dish and one other untreated dish for each of the eight cell lines were harvested for gene expression analyses. Cells from the third untreated dish for each cell line were harvested for TL measurement.

Quantitative real-time PCR

For mRNA quantification, total RNA was isolated using a standard extraction kit (Macherey-Nagel NucleoSpin RNA, catalog no. 740955) and quantified with a NanoDrop ND 1000 spectrophotometer. Complementary DNA (cDNA) synthesis was carried out following the manufacturer's instructions [M-MLV Reverse Transcriptase, RNase (H−), Promega, catalog no. M5301]. One microgram of mRNA was used for the reverse transcriptase reaction.

qPCR was carried out using TaqMan Universal Master Mix II, no. UNG (catalog no. 4440040) from Applied Biosystems and following the manufacturer's manual. The cDNA samples (5 ng/μl) were assayed in triplicate; the nontemplate control (water) was analyzed in duplicate in a 384-well plate. The assay was carried out using a Bio-Rad CFX384 real-time C1000 thermal cycler with the following thermal cycling profile: 10 min at 95°C, followed by 50 cycles at 95°C for 15 s and 1 min at 60°C with signal acquisition. For gene expression quantification of the potential TPE and control genes, the gene expression TaqMan assays from Applied Biosystems were used. Primer characteristics are summarized in table S7. The ΔΔCt method was used for relative quantification. The relative expression level of each gene was normalized to its level in untreated low-PD cells. The mean and SEM were calculated from technical duplicates or triplicates of biological replicates.

TL measurement

A standard extraction kit (DNeasy Blood & Tissue Kit, Qiagen, catalog no. 69504) was used for DNA extraction. Mean TL was determined using the modified MMqPCR method as described previously (*73*). This technique enables telomere-specific and single-copy gene (reference) amplification in a single reaction well with quantification measurements at different temperatures. The ratio of telomere to single-copy gene content (TLR) is taken as a relative measure of TL and is expressed in arbitrary units. The DNA samples (20 ng/μl, as a single copy) and a reference DNA standard (186.6 to 0.09 ng) were assayed in triplicate on different plates. A nontemplate control (water) and positive control (human leukemia cell line 1301 DNA) were prepared in duplicate and run on every plate. The assay was performed using a Bio-Rad CFX384 real-time C1000 thermal cycler with the following thermal cycling profile: 1 cycle of 15 min at 95°C; 2 cycles of 15 s at 94°C; 1 cycle of 15 s at 49°C; 40 cycles of 15 s at

94°C; 1 cycle 10 s at 62°C; and 1 cycle 15 s at 72°C with T signal acquisition, 10 s at 85°C, and 15 s at 89°C with signal acquisition. The reagents for PCR were used at the following final concentrations: 1 U of titanium Taq DNA polymerase per reaction with the provided titanium Taq PCR buffer (catalog no. 639208), 0.75× SYBR Green I (Sigma-Aldrich), 0.2 mM of each deoxynucleotide triphosphate, 1 mM dithiothreitol, 1 M betaine, 900 nM of each telomere primer (telg and telc), and 300 nM of each single-copy gene primer (albu and albd). Primer sequences are shown in table S7.

All samples were measured in triplicate, and the average of the three measurements was used to report the mean TL for each sample. The intra-assay coefficients of variation were <0.3 for all samples.

SA-β-Gal staining

The four HGP patient fibroblast cell lines and two control cell lines (731 and/or 811) were used for SA-β-Gal staining. Determination of β-galactosidase activity was performed using a histochemical staining kit from Sigma-Aldrich (catalog no. CS0030). The procedure was performed according to the manufacturer's recommendations. Briefly, cells were transferred into two wells of a 12-well plate and cultivated in fibroblast medium for approximately 1 day (to approximately 50 to 70% confluence). Cells in one well were treated with 200 μM H_2O_2 in 2 ml of fibroblast medium for 1.5 hours, washed with 1 ml of PBS, and incubated for another 4 hours in fibroblast medium followed by staining. Untreated cells were stained in the absence of H_2O_2. For the staining procedure, the cells were first washed twice with 1 ml of PBS per well and then fixed for 6 to 7 min at room temperature (RT) with 500 μl of 1× fixation buffer [10× fixation buffer (catalog no. F1797) diluted with H_2O]. The final concentrations in the cell dishes were 2% formaldehyde, 0.2% glutaraldehyde, 7.04 mM Na_2HPO_4, 1.47 mM KH_2PO_4, 0.13 M NaCl, and 2.68 mM KCl. Continuing the staining procedure, the cells were then washed again three times with 1 ml per well of PBS and incubated overnight at 37°C without CO_2 in 500 μl of staining mixture [10× staining solution (catalog no. S5818), reagent B (catalog no. R5272), reagent C (catalog no. R5147), X-gal solution (catalog no. X3753)]. The staining mixture was filtered through a 0.2-μm filter before use to remove aggregates. The percentage of SA-β-Gal–positive cells was ascertained by counting all visible cells in four fields of view of a light microscope at ×50 magnification. The counting was performed independently by two different individuals who were blinded to the treatment. Four dishes were excluded from analysis because of complete cell death after H_2O_2 treatment. The mean and SD were formed by using technical duplicates and biological replicates.

MUG assay

The four HGP patient fibroblast cell lines and two control cell lines (731 and/or 811) were used for the MUG assay. This highly sensitive spectrophotometric method is an alternative for SA-β-Gal staining and subjective visual quantification that measures enzyme activity in cell lysates (*69*). In this assay, β-galactosidase acts on the substrate MUG to produce 4-methylumbelliferone galactosidase, which can be detected fluorometrically (*74*). For each cell line, approximately 3.2×10^6 cells were transferred into two 5-cm culture dishes (i.e., ca. 1.6×10^6 cells per dish) and were cultivated to 50 to 70% confluence. One dish of each cell line was treated with 200 μM H_2O_2 in 3 ml of fibroblast medium for 1.5 hours and then incubated in normal fibroblast medium for another 4 hours. The following steps were executed according to the protocol by Gary and Kindell (*75*). The cells were washed six times with 1 ml of PBS, lysed with 200 μl of lysis buffer [5 mM CHAPS, 40 mM citric acid, and 40 mM sodium phosphate (pH 6)], and transferred into 1.5-ml Eppendorf tubes using a cell scraper. The cells were vortexed for 20 s and centrifuged at 12,000*g* for 5 min at RT. The supernatant was frozen at 20°C until analysis. For measurements, 100 μl of the lysate was transferred into a reaction tube and mixed with 50 μl of lysis buffer and 150 μl of 2× reaction buffer [40 mM citric acid, 40 mM sodium phosphate, 300 mM NaCl, 10 mM mercaptoethanol, and 4 mM $MgCl_2$ (pH 6), stored at 4°C]; 1.7 mM MUG (Sigma-Aldrich, catalog no. M1633, stored at −20°C) was added immediately before use. The reaction solution was incubated for 3 hours at 37°C. After 3 hours, 50 μl of the reaction solution was withdrawn and transferred to a new Eppendorf tube containing 500 μl of stopping solution (400 mM Na_2CO_3) to inhibit the enzymatic reaction. Then, 150 μl of the solution was transferred into a well of a 96-well plate. Fluorescence was measured in duplicate with Fluoroskan Ascent FL (Thermo Fisher Scientific) at 360-nm excitation and 465-nm emission. The protein concentration of the lysate was determined using bicinchoninic acid (BCA) assay (with human albumin as the standard), and the fluorescence signal was normalized to the total protein concentration. Typical concentrations were in the range of 0.3 to 1.0 μg/ml. The results are displayed as relative fluorescence units per milligram (RFU/mg). The mean and SD were calculated from technical duplicates of biological replicates.

Western blotting

Fibroblast cell lines grown to confluence in a 7-cm dish (~5×10^6 cells) were washed with 5 ml of 0.1% EDTA/PBS and then detached with 400 μl of trypsin/EDTA (Gibco, catalog no. 25200-056). The cells were removed in 7 ml of fibroblast medium and centrifuged at 1200*g* for 5 min at RT. The supernatant was discarded, and the pellet was resuspended in 1 ml of PBS, transferred to a 1.5-ml Eppendorf tube, and centrifuged again at 1200*g* for 5 min. The supernatant was discarded, and the cells were resuspended in 200 μl of sucrose-Hepes buffer [SHC buffer; 0.2 M sucrose, 0.02 M Hepes (pH 7.3), and cOmplete ULTRA Tablets EDTA-free (Roche, catalog no. 05 892 791 001)] and lysed by pipetting the cell suspension up and down 10 times in a syringe through a 26G insulin injection needle. After 10-s centrifugation at 6000*g* to remove unlysed cell debris, the supernatant was aliquoted into Eppendorf tubes and stored at −80°C until analysis.

Protein concentrations were measured using the Pierce BCA Protein Assay Kit (Thermo Fisher Scientific, catalog no. 23225) with albumin as the standard. Then, 15 μg of the cell homogenate was mixed with 2× sample buffer [0.1 M tris (pH 6.8), 8% (w/v) SDS, 40% (w/v) glycerin, bromophenol blue (0.2 mg/ml), and 20% β-mercaptoethanol]. SDS–polyacrylamide gel electrophoresis was performed with 7.5 and 10% polyacrylamide gels. The gels were transferred to polyvinylidene fluoride membranes (Millipore, catalog no. IPVH00010).

The membranes were incubated with primary antibodies against phospho-p70 S6 kinase (Thr^{389}) (108D2) rabbit monoclonal antibody (mAb) (Cell Signaling Technology, catalog no. 9234) (1:2000), phospho-mTOR (Ser^{2448}) (D9C2) XP rabbit mAb (Cell Signaling Technology, catalog no. 5536) (1:1000), and phospho-Akt (Ser^{473}) rabbit mAb (Cell Signaling Technology, catalog no.9271) (1:1000), all diluted in BSA-blocking solution [5% BSA, 0.1% Tween 20, 20 mM tris, and 0.15 M NaCl (pH 7.5)], overnight at 4°C. The membranes were then incubated with goat anti-rabbit IgG (H + L)–horseradish peroxidase (HRP)–conjugated (Bio-Rad, catalog no. 1706515) (1:5000)

secondary antibody for 1 hour at RT. Blots were exposed to CL-XPosure Films (Thermo Fisher Scientific, catalog no. 34089) with a homemade enhanced chemiluminescence (ECL) solution using 2 ml of solution A [50 mg of luminol (Fluka, catalog no. 09253) in 200 ml 0.1 M tris solution (pH 8.6)] and 0.2 ml solution B [11 mg of para-coumaric acid (Sigma-Aldrich, catalog no. 501-98-4) in 10 ml of dimethyl sulfoxide (DMSO)] supplemented with 1 μl of 30% H_2O_2 before use for each membrane. All blots were stripped with glycine stripping buffer (100 mM glycine and 320 mM HCl) for 30 min at 60°C.

Membranes were incubated overnight at 4°C with primary antibodies against p70 S6 kinase clone 20-10C-6, rabbit mAb (Millipore, catalog no. 05-781R) (1:6000); mTOR (7C10) rabbit mAb (Cell Signaling Technology, catalog no. 2983) (1:1000); Akt (C-20) (Santa Cruz Biotechnology, catalog no. sc-1618) (1:500); and mouse monoclonal anti–β-actin (clone AC-15, Sigma-Aldrich, catalog no. A5441) (1:80,000), all of which were diluted in milk-blocking solution [5% skimmed milk powder, 0.1% Tween 20, 20 mM tris, and 0.15 M NaCl (pH 7.5)]. As secondary antibodies, we used goat anti-mouse IgG (H + L)–HRP conjugate (Bio-Rad, catalog no. 1706516), goat anti-rabbit IgG (H + L)–HRP conjugate (Bio-Rad, catalog no. 1706515), rabbit anti-goat immunoglobulins, and polyclonal HRP (DakoCytomation, catalog no. P0449) at a dilution of 1:40,000 for β-actin and 1:5000 for all others. Incubation time was 1 hour at RT. Blots were developed as described above.

For ARSA experiments, the membranes were incubated overnight at 4°C with human anti-ARSA/ARSA antibody (R&D Systems, catalog no.MAB2485) (1:1000) diluted in milk-blocking solution, as described above. The secondary antibody goat anti-mouse IgG (H + L)–HRP conjugate (Bio-Rad, catalog no. 1706516) (1:5000) was incubated for 1 hour. Blots were exposed to CL-XPosure Films (Thermo Fisher Scientific, catalog no. 34089) on SuperSignal West Femto Maximum Sensitivity Substrate (Thermo Fisher Scientific, catalog no. 34096). Blots were stripped and incubated with monoclonal anti–β-actin antibody as described above.

Densitometric analysis was performed using Image Studio Lite Quantification Software (LI-COR). The mean and SEM values were calculated from biological quadruplicates and technical replicates, all normalized to β-actin.

Three-dimensional fluorescence in situ hybridization

Three fibroblast cell lines of patients with HGP (HGADFN127, HGADFN164, and HGADFN178) and three control cell lines (707, 731, and 778) were used for 3D-FISH experiments. Cell pairs with short and long telomeres were used for 3D-FISH analyses. Fibroblasts were cultivated in a T25 flask until they reached 100% confluence. The cells were then trypsinized and centrifuged, and the cell pellets were solubilized in PBS.

For slide preparation, cells were treated following established protocols for direct cell nucleus preparation. Briefly, the cell suspension was mixed carefully with 0.9% NaCl in a 1:1 ratio. After 10-min centrifugation at 210*g* at RT, the supernatant was discarded, and the cell pellet was incubated with 5 ml of 0.4% KCl solution (preheated to 37°C) for 10 min at RT. Then, 2 ml of ice-cold fixing solution (methanol/acetic acid 3 + 1) was added, and the whole mixture was centrifuged again.

The pelleted cells were fixed in 5 ml of ice-cold fixing solution. First, 1 ml of fixation solution was added dropwise and carefully mixed. The rest of the fixation solution was then slowly added and carefully mixed again. The fixing solution was changed five times immediately. Last, the supernatant was aspirated and the cell pellet was resuspended. After fixation, 10 μl of cell suspension was carefully dropped onto a slide, incubated for 15 min at 80°C on a heating plate, and washed briefly with PBS. For pepsin digestion, slides were incubated with pepsin solution [50 μl of pepsin (Sigma-Aldrich, catalog no. 1.07192.001) and 100 ml of 0.01 N HCl] for 10 min at 37°C. The slides were washed with PBS and then incubated for 3 min with PBS/$MgCl_2$. The slides were then incubated for 10 min with 1% formaldehyde, followed by 3 min with PBS at RT and then 2 min at RT in ascending ethanol (70–85–100%); last, the slides were dried at RT.

For hybridization, 2 μl of probe was added to the hybridization field. The Vysis TelVysion 4p spectrum probe (Abbott, Vysis, catalog no. 30-252004) was used for detection of the 4p subtelomeric region. For detection of the *PPP2R2C* region on the chromosome, RP11-462B2 BAC (Illumina) labeled with Spectrum Orange was used. Slides were then covered carefully with a cover glass and sealed with Fix-O-Gum (Marabu, catalog no. 29010017000). The codenaturation step was carried out for 5 min at 80°C on a heating plate. The slide was then incubated for 24 hours in a 37°C water bath protected from light. For the final washing step, the cover glass was removed carefully, and the slides were incubated for 2 min in 0.4× SSC/0.3% IGEPAL® CA-630 (Sigma-Aldrich, catalog no. 13021) solution at 73°C, briefly washed with 2× SSC/0.1% IGEPAL solution, and then washed with PBS at RT. The ethanol series described above was repeated, and the slides were air-dried. One drop of Vectashield/4′,6-diamidino-2-phenylindole (DAPI) mixture (Vectashield, Vector, #H-1000; DAPI, Sigma-Aldrich, catalog no. 10236276001) was pipetted onto the slides and covered with a cover glass.

Images were acquired with a confocal scanning laser microscope (LSM 880 AxioExaminer Z1 from Zeiss) using 405-nm excitation/415- to 480-nm emission for DAPI, 488-nm excitation/500- to 545-nm emission for Spectrum Green, and 561-nm excitation/565- to 640-nm emission for Spectrum Orange. A 63× numerical aperture 1.4 Plan-Apochromat oil immersion objective was used to capture optical sections at intervals of 0.3 mm. The pinhole was set to about 1 airy unit to achieve optical slices at all wavelengths with identical thickness. Images were then processed using Imaris 9.3 software (Andor Bitplane). A total of 70 cell nuclei (140 distances) were analyzed for each experiment. Cells with fewer or more than four signals (two red and two green signals each), irregular DAPI staining (e.g., mitotic cells), and abnormal cell shape were excluded from further analysis (excluded data points are available on request). The distance between their gravity centers (distance between the closest probes in each target) was determined by 3D reconstruction and surface rendering of the spots and used for further statistical analysis.

Binary and ordinal data are shown as absolute numbers and percentages. Continuous variables are displayed as the mean (SD) when normally distributed and the median (range) when not normally distributed. As the distance between the gravity centers after 3D reconstruction in the nuclei was not normally distributed, log transformation of both distances (AB and CD) was applied. Hierarchical linear models were used to estimate the impact of immortalization on the distance between gravity centers. We allowed random variation between cells, and cells were nested within cell lines. The results are displayed together with their *P* values and 95% confidence intervals (table S6). Distances were divided into deciles (0.7258, 1.090, 1.3442, 1.606, 1.93, 2.28, 2.773, 3.49, and 4.451 μm) for graphical presentation (figs. S8, C, and D, and S9). To evaluate the optimal cut

point for the distinction between cells with or without immortalization (Fig. 4 and fig. S8, A and B), the R package "OptimalCutpoints" (*76*) was used. The optimal cut point was 2.26 μm. The area under the curve with this cut point was 0.63 with a sensitivity of 52% and a specificity of 69%.

PPP2R2C knockdown via 27-mer siRNA duplex

The knockdown of *PPP2R2C* was conducted using the Trilencer-27 Human siRNA Kit (OriGene; SR303688). The provided siRNAs were mixed to maximize knock-down efficiency. Cells were grown in DMEM containing 10% FBS (Biochrome), penicillin (100 U/ml), and streptomycin (100 μg/ml) (Biochrome, catalog no. A2212) in T25 flasks.

Primary cells of the cell line HGADFN127 were used at high PD for this experiment.

When cells reached a confluence of approximately 80%, siRNAs was added to a final concentration of 25 or 50 nM in the medium, following the instructions provided by the manufacturer. siRNA-containing medium was replaced by normal medium as soon as the cells started to show signs of cellular stress (7 hours). Cells were harvested 72 hours after removal of siRNA-containing medium and lysed for protein and mRNA isolation as described above.

Serum deprivation

For serum deprivation experiments, the 811 primary and *hTERT* immortalized cell lines were used. Cells were grown in two T75 flasks and treated at ~95% confluence for 18 hours in DMEM without pyruvate supplemented with 10% FBS and penicillin (100 U/ml) and streptomycin (100 μg/ml), and for 17 hours in DMEM supplemented with 10% FBS, and then 1 hour only in PBS. Cells were harvested for protein and RNA isolation as described. The cDNA samples (5 ng/μl) were assayed in triplicate; the nontemplate control (water) was analyzed in duplicate in a 384-well plate. For gene expression quantification, the following TaqMan assays were used: *PPP2R2C* (Applied Biosystems, catalog no. Hs00902099_m1) and *mTOR* (Applied Biosystems, catalog no. Hs00234508_m1). Human *PPIA* (*cyclophilin A*) (Applied Biosystems, catalog no. 4333763F) was used as the endogenous control. The ΔΔCt method was used for relative quantification.

Inhibitor tests

Three fibroblast cell lines from healthy individuals (707, 731, and 778) were used for TSA/5-AzaC and RSV experiments. TSA inhibits histone deacetylases (*33*). 5-AzaC results in nonspecific overall DNA demethylation (*34*) and RSV induces instability of telomeric DNA (*35*).

For TSA and 5-AzaC treatment, cells were grown in four 100 mm by 20 mm tissue culture dishes (Falcon, catalog no. 353003), denoted by letters A to D, from 25% initial confluence to 70% final confluence (A to D; A: DMSO control, B: TSA only; C: 5-AzaC only; D: TSA and 5-AzaC). 5-AzaC (1 μg/ml; Sigma-Aldrich, catalog no. A2385) dissolved in full medium was added to dishes C and D. The cells were then incubated in 5% CO_2 for 48 hours at 37°C. After 48 hours of incubation, TSA (0.2 μg/ml) (Sigma-Aldrich, catalog no. T8552) dissolved in DMSO was added to dishes B and D. To control for nonspecific DMSO side effects and to create comparable conditions, DMSO was added to dishes A and C at this time point. After 24 hours of incubation, the old medium was discarded, and fresh medium was added. After another 24 hours of equilibration incubation, the mRNA was isolated, and qPCR was performed as described.

For RSV treatment, cells were grown in four wells (A, B, C, and D) of a six-well tissue culture plate (Falcon, catalog no. 353046) and incubated in 5% CO_2 for 24 hours at 37°C. RSV (Merck, catalog no. 554325) in DMSO was added to fresh medium at different concentrations: A: 0 μM RSV (DMSO-only control); B: 0.25 μM RSV; C: 1.0 μM RSV; and D: 10 μM RSV. After a total 48-hour incubation, mRNA was isolated, and qPCR was performed.

The healthy cell line 778 was used for SIRT6 inhibitor treatment. Compound BCI-150 is a recently developed SIRT inhibitor with selectivity for SIRT6 versus SIRT1 and SIRT2 (*38*). Cells were grown in two wells (A and B) of a six-well tissue culture plate and incubated in 5% CO_2 for 24 hours at 37°C. Subsequently, the SIRT6 inhibitor BCI-150 (Asiner Ltd., catalog no. SYN 17739303), a gift from A. Del Rio (Institute of Organic Synthesis and Photoreactivity, National Council, Bologna, Italy), was added to well B at a concentration of 50 μM (in DMSO) in fresh medium. Only DMSO was added to well A (control). The cells were incubated for another 48 hours; mRNA was isolated as described above, and qPCR was performed.

qPCR was carried out using TaqMan Universal Master Mix II, no UNG (catalog no. 4440040) from Applied Biosystems following the manufacturer's manual. The cDNA samples (5 ng/μl) were assayed in triplicate; the nontemplate control (water) was analyzed in duplicate in a 384-well plate. The assay was carried out using a Bio-Rad CFX384 real-time C1000 thermal cycler with the following thermal cycling profile: 10 min at 95°C, followed by 50 cycles at 95°C for 15 s and 1 min at 60°C with signal acquisition. For gene expression quantification of the potential TPE gene *PPP2R2C*, a TaqMan assay (Applied Biosystems, catalog no. Hs00902099_m1) was used. Human *PPIA* (*cyclophilin A*) (Applied Biosystems, catalog no. 4333763F) was used as the endogenous control. The ΔΔCt method was used for relative quantification. The relative expression level of each gene was normalized to that of the youngest cells (low PD) treated with DMSO.

Distribution of cells in the growth phase

Fibroblasts were cultivated on 100 mm by 20 mm tissue culture dishes (Falcon, catalog no. 353003) to ~70 to 80% confluence. For cell synchronization, cells were cultivated for 24 hours with DMEM/1% penicillin/streptomycin and 0.1% fetal calf serum. After 24 hours, the cells were harvested and prepared for cell cycle analyses. The cell pellets were resuspended in 500 μl of 70% ethanol and incubated at 4°C for 24 hours. The cells were centrifuged and resuspended in 200 μl of PBS with propidium iodide (50 μg/ml) (Sigma-Aldrich, catalog no. 25535-16-4) and ribonuclease A (25 μl/ml) (Macherey-Nagel, catalog no. 740505.50) and then incubated in the dark at RT for 30 min. The cell suspension was added to a fluorescence-activated cell sorting (FACS) Falcon and filled with 200 μl of PBS. Ten thousand cells were counted for routine FACS analyses (FACSCalibur).

Arylsulfatase activity

The arylsulfatase, an enzyme activity in protein homogenates, was determined following a modified protocol according to Böhringer *et al.* (*77*). For this purpose, 25 μg of total protein isolated as described in (*78*) was diluted in 50 μl of SHC buffer and 50 μl of reaction buffer [10 mM 4-nitrocatechosulfate, 10% (w/v) NaCl, 0.3% (v/v) Triton X-100 (Sigma-Aldrich), and bovine serum albumin (1 mg/ml; Sigma-Aldrich)], in 0.5 M sodium acetate (pH 5.0) was added, followed by incubation at 37°C for 6 hours. The reaction was terminated by adding 800 μl of stop buffer (1 M NaOH), and the 4-nitrocatechol

released by ARSA was assessed at 515 nm using a spectrophotometer (Pharmacia Biotech) against water. As a blank, a similar assay was immediately stopped with 250 µl of 0.5 N NaOH and absorption read again. The difference between absorptions read for reacted and blank assay was transformed to the activity unit pmol nitrocatecholsulfate degraded per minute.

Other statistical analysis

The package OptimalCutpoints in R 3.6.1 (*79*) was used for all scatter diagrams and for 3D-FISH cut point analysis. The code for data retrieval for scatter diagrams and heat maps is available at https://bitbucket.org/ibima/tpe-old and was programmed with R 3.6.1 (*79*). Statistical analyses were conducted using OriginPro 2018 and SPSS for Windows (IBM Corp. Released 2017. IBM SPSS Statistics for Windows, Version 25.0. Armonk, NY: IBM Corp). Normally distributed variables are shown as the means ± SD or as the SEM as indicated. The two-sided exact Mann-Whitney *U* test was applied to evaluate differences between two independent groups in non-normally distributed variables. $P < 0.05$ was considered statistically significant.

SUPPLEMENTARY MATERIALS

Supplementary material for this article is available at https://science.org/doi/10.1126/sciadv.abk2814

View/request a protocol for this paper from *Bio-protocol*.

REFERENCES AND NOTES

1. J. W. Shay, W. E. Wright, Telomeres and telomerase: Three decades of progress. *Nat. Rev. Genet.* **20**, 299–309 (2019).
2. J. Campisi, Senescent cells, tumor suppression, and organismal aging: Good citizens, bad neighbors. *Cell* **120**, 513–522 (2005).
3. J. W. Shay, Role of telomeres and telomerase in aging and cancer. *Cancer Discov.* **6**, 584–593 (2016).
4. C. B. Harley, A. B. Futcher, C. W. Greider, Telomeres shorten during ageing of human fibroblasts. *Nature* **345**, 458–460 (1990).
5. J. Maciejowski, T. de Lange, Telomeres in cancer: Tumour suppression and genome instability. *Nat. Rev. Mol. Cell Biol.* **18**, 175–186 (2017).
6. J. A. Hackett, C. W. Greider, Balancing instability: Dual roles for telomerase and telomere dysfunction in tumorigenesis. *Oncogene* **21**, 619–626 (2002).
7. M. A. Blasco, H. W. Lee, M. P. Hande, E. Samper, P. M. Lansdorp, R. A. DePinho, C. W. Greider, Telomere shortening and tumor formation by mouse cells lacking telomerase RNA. *Cell* **91**, 25–34 (1997).
8. J. A. Baur, Y. Zou, J. W. Shay, W. E. Wright, Telomere position effect in human cells. *Science* **292**, 2075–2077 (2001).
9. J. D. Robin, A. T. Ludlow, K. Batten, M. C. Gaillard, G. Stadler, F. Magdinier, W. E. Wright, J. W. Shay, SORBS2 transcription is activated by telomere position effect-over long distance upon telomere shortening in muscle cells from patients with facioscapulohumeral dystrophy. *Genome Res.* **25**, 1781–1790 (2015).
10. J. D. Robin, A. T. Ludlow, K. Batten, F. Magdinier, G. Stadler, K. R. Wagner, J. W. Shay, W. E. Wright, Telomere position effect: Regulation of gene expression with progressive telomere shortening over long distances. *Genes Dev.* **28**, 2464–2476 (2014).
11. Z. Lou, J. Wei, H. Riethman, J. A. Baur, R. Voglauer, J. W. Shay, W. E. Wright, Telomere length regulates ISG15 expression in human cells. *Aging* **1**, 608–621 (2009).
12. W. Kim, A. T. Ludlow, J. Min, J. D. Robin, G. Stadler, I. Mender, T.-P. Lai, N. Zhang, W. E. Wright, J. W. Shay, Regulation of the human telomerase gene *TERT* by telomere position effect-over long distances (TPE-OLD): Implications for aging and cancer. *PLoS Biol.* **14**, e2000016 (2016).
13. M. L. Decker, E. Chavez, I. Vulto, P. M. Lansdorp, Telomere length in Hutchinson-Gilford progeria syndrome. *Mech. Ageing Dev.* **130**, 377–383 (2009).
14. Y. Li, G. Zhou, I. G. Bruno, J. P. Cooke, Telomerase mRNA reverses senescence in progeria cells. *J. Am. Coll. Cardiol.* **70**, 804–805 (2017).
15. L. B. Gordon, F. G. Rothman, C. López-Otín, T. Misteli, Progeria: A paradigm for translational medicine. *Cell* **156**, 400–407 (2014).
16. N. Wlodarchak, Y. Xing, PP2A as a master regulator of the cell cycle. *Crit. Rev. Biochem. Mol. Biol.* **51**, 162–184 (2016).
17. M. Kiely, P. A. Kiely, PP2A: The wolf in sheep's clothing? *Cancer* **7**, 648–669 (2015).
18. N. M. V. Gomes, O. A. Ryder, M. L. Houck, S. J. Charter, W. Walker, N. R. Forsyth, S. N. Austad, C. Venditti, M. Pagel, J. W. Shay, W. E. Wright, Comparative biology of mammalian telomeres: Hypotheses on ancestral states and the roles of telomeres in longevity determination. *Aging Cell* **10**, 761–768 (2011).
19. ELIXIR, *g:Profiler, version e104_eg51_p15_3922dba; organism: hsapiens* (2 June 2021); https://biit.cs.ut.ee/gprofiler/gost.
20. J. Reimand, M. Kull, H. Peterson, J. Hansen, J. Vilo, g:Profiler--a web-based toolset for functional profiling of gene lists from large-scale experiments. *Nucleic Acids Res.* **35**, W193–W200 (2007).
21. Y.-L. Fan, L. Chen, J. Wang, Q. Yao, J.-Q. Wan, Over expression of PPP2R2C inhibits human glioma cells growth through the suppression of mTOR pathway. *FEBS Lett.* **587**, 3892–3897 (2013).
22. H.-H. Li, X. Cai, G. P. Shouse, L. G. Piluso, X. Liu, A specific PP2A regulatory subunit, B56γ, mediates DNA damage-induced dephosphorylation of p53 at Thr55. *EMBO J.* **26**, 402–411 (2007).
23. Z. Yan, S. A. Fedorov, M. C. Mumby, R. S. Williams, PR48, a novel regulatory subunit of protein phosphatase 2A, interacts with Cdc6 and modulates DNA replication in human cells. *Mol. Cell. Biol.* **20**, 1021–1029 (2000).
24. S. Yu, L. Li, Q. Wu, N. Dou, Y. Li, Y. Gao, PPP2R2D, a regulatory subunit of protein phosphatase 2A, promotes gastric cancer growth and metastasis via mechanistic target of rapamycin activation. *Int. J. Oncol.* **52**, 2011–2020 (2018).
25. Y. Zhao, A. Tyshkovskiy, D. Muñoz-Espín, X. Tian, M. Serrano, J. P. de Magalhaes, E. Nevo, V. N. Gladyshev, A. Seluanov, V. Gorbunova, Naked mole rats can undergo developmental, oncogene-induced and DNA damage-induced cellular senescence. *Proc. Natl. Acad. Sci. U.S.A.* **115**, 1801–1806 (2018).
26. T. Cindrova-Davies, N. M. E. Fogarty, C. J. P. Jones, J. Kingdom, G. J. Burton, Evidence of oxidative stress-induced senescence in mature, post-mature and pathological human placentas. *Placenta* **68**, 15–22 (2018).
27. J. R. Baker, C. Vuppusetty, T. Colley, A. I. Papaioannou, P. Fenwick, L. Donnelly, K. Ito, P. J. Barnes, Oxidative stress dependent microRNA-34a activation via PI3Kα reduces the expression of sirtuin-1 and sirtuin-6 in epithelial cells. *Sci. Rep.* **6**, 35871 (2016).
28. A. Ottaviani, E. Gilson, F. Magdinier, Telomeric position effect: From the yeast paradigm to human pathologies? *Biochimie* **90**, 93–107 (2008).
29. Y. Sakakibara, M. Sekiya, N. Fujisaki, X. Quan, K. M. Iijima, Knockdown of *wfs1*, a fly homolog of Wolfram syndrome 1, in the nervous system increases susceptibility to age- and stress-induced neuronal dysfunction and degeneration in *Drosophila*. *PLOS Genet.* **14**, e1007196 (2018).
30. E. Machiela, R. Jeloka, N. S. Caron, S. Mehta, M. E. Schmidt, H. J. E. Baddeley, C. M. Tom, N. Polturi, Y. Xie, V. B. Mattis, M. R. Hayden, A. L. Southwell, The interaction of aging and cellular stress contributes to pathogenesis in mouse and human huntington disease neurons. *Front. Aging Neurosci.* **12**, 524369 (2020).
31. D. M. Baird, J. Rowson, D. Wynford-Thomas, D. Kipling, Extensive allelic variation and ultrashort telomeres in senescent human cells. *Nat. Genet.* **33**, 203–207 (2003).
32. R. J. O'Sullivan, S. Kubicek, S. L. Schreiber, J. Karlseder, Reduced histone biosynthesis and chromatin changes arising from a damage signal at telomeres. *Nat. Struct. Mol. Biol.* **17**, 1218–1225 (2010).
33. P. A. Marks, V. M. Richon, R. A. Rifkind, Histone deacetylase inhibitors: Inducers of differentiation or apoptosis of transformed cells. *J. Natl. Cancer Inst.* **92**, 1210–1216 (2000).
34. V. M. Komashko, P. J. Farnham, 5-Azacytidine treatment reorganizes genomic histone modification patterns. *Epigenetics* **5**, 229–240 (2010).
35. M. Rusin, A. Zajkowicz, D. Butkiewicz, Resveratrol induces senescence-like growth inhibition of U-2 OS cells associated with the instability of telomeric DNA and upregulation of BRCA1. *Mech. Ageing Dev.* **130**, 528–537 (2009).
36. W. Dang, K. K. Steffen, R. Perry, J. A. Dorsey, F. B. Johnson, A. Shilatifard, M. Kaeberlein, B. K. Kennedy, S. L. Berger, Histone H4 lysine 16 acetylation regulates cellular lifespan. *Nature* **459**, 802–807 (2009).
37. R. I. Tennen, D. J. Bua, W. E. Wright, K. F. Chua, SIRT6 is required for maintenance of telomere position effect in human cells. *Nat. Commun.* **2**, 433 (2011).
38. M. D. Parenti, A. Grozio, I. Bauer, L. Galeno, P. Damonte, E. Millo, G. Sociali, C. Franceschi, A. Ballestrero, S. Bruzzone, A. Del Rio, A. Nencioni, Discovery of novel and selective SIRT6 inhibitors. *J. Med. Chem.* **57**, 4796–4804 (2014).
39. Q. P. Weng, M. Kozlowski, C. Belham, A. Zhang, M. J. Comb, J. Avruch, Regulation of the p70 S6 kinase by phosphorylation in vivo. Analysis using site-specific anti-phosphopeptide antibodies. *J. Biol. Chem.* **273**, 16621–16629 (1998).
40. X. Wang, P. Yue, H. Tao, S.-Y. Sun, Inhibition of p70S6K does not mimic the enhancement of Akt phosphorylation by rapamycin. *Heliyon* **3**, e00378 (2017).
41. J. F. Gera, I. K. Mellinghoff, Y. Shi, M. B. Rettig, C. Tran, J. H. Hsu, C. L. Sawyers, A. K. Lichtenstein, AKT activity determines sensitivity to mammalian target of rapamycin (mTOR) inhibitors by regulating cyclin D1 and c-myc expression. *J. Biol. Chem.* **279**, 2737–2746 (2004).
42. V. Gire, V. Dulic, Senescence from G2 arrest, revisited. *Cell Cycle* **14**, 297–304 (2015).

43. L. Bertram, A. Böckenhoff, I. Demuth, S. Düzel, R. Eckardt, S. C. Li, U. Lindenberger, G. Pawelec, T. Siedler, G. G. Wagner, E. Steinhagen-Thiessen, Cohort profile: The Berlin Aging Study II (BASE-II). *Int. J. Epidemiol.* **43**, 703–712 (2014).
44. S. Herwest, C. Albers, M. Schmiester, B. Salewsky, W. Hopfenmüller, A. Meyer, L. Bertram, I. Demuth, The hSNM1B/Apollo variant rs11552449 is associated with cellular sensitivity towards mitomycin C and ionizing radiation. *DNA Repair* **72**, 93–98 (2018).
45. D. Eckert, S. Buhl, S. Weber, R. Jäger, H. Schorle, The AP-2 family of transcription factors. *Genome Biol.* **6**, 246 (2005).
46. K. Beishline, J. Azizkhan-Clifford, Sp1 and the 'hallmarks of cancer'. *FEBS J.* **282**, 224–258 (2015).
47. M. M. Ouellette, L. D. McDaniel, W. E. Wright, J. W. Shay, R. A. Schultz, The establishment of telomerase-immortalized cell lines representing human chromosome instability syndromes. *Hum. Mol. Genet.* **9**, 403–411 (2000).
48. E. G. Bluemn, E. S. Spencer, B. Mecham, R. R. Gordon, I. Coleman, D. Lewinshtein, E. Mostaghel, X. Zhang, J. Annis, C. Grandori, C. Porter, P. S. Nelson, PPP2R2C loss promotes castration-resistance and is associated with increased prostate cancer-specific mortality. *Mol. Cancer Res.* **11**, 568–578 (2013).
49. J. Zhang, Z. Gao, J. Ye, Phosphorylation and degradation of S6K1 (p70S6K1) in response to persistent JNK1 Activation. *Biochim. Biophys. Acta* **1832**, 1980–1988 (2013).
50. A. A. Khan, D. Betel, M. L. Miller, C. Sander, C. S. Leslie, D. S. Marks, Transfection of small RNAs globally perturbs gene regulation by endogenous microRNAs. *Nat. Biotechnol.* **27**, 549–555 (2009).
51. M. Ogrodnik, H. Salmonowicz, D. Jurk, J. F. Passos, Expansion and cell-cycle arrest: Common denominators of cellular senescence. *Trends Biochem. Sci.* **44**, 996–1008 (2019).
52. M. V. Blagosklonny, Geroconversion: Irreversible step to cellular senescence. *Cell Cycle* **13**, 3628–3635 (2014).
53. C. Selman, J. M. A. Tullet, D. Wieser, E. Irvine, S. J. Lingard, A. I. Choudhury, M. Claret, H. Al-Qassab, D. Carmignac, F. Ramadani, A. Woods, I. C. A. Robinson, E. Schuster, R. L. Batterham, S. C. Kozma, G. Thomas, D. Carling, K. Okkenhaug, J. M. Thornton, L. Partridge, D. Gems, D. J. Withers, Ribosomal protein S6 kinase 1 signaling regulates mammalian life span. *Science* **326**, 140–144 (2009).
54. D. E. Harrison, R. Strong, Z. D. Sharp, J. F. Nelson, C. M. Astle, K. Flurkey, N. L. Nadon, J. E. Wilkinson, K. Frenkel, C. S. Carter, M. Pahor, M. A. Javors, E. Fernandez, R. A. Miller, Rapamycin fed late in life extends lifespan in genetically heterogeneous mice. *Nature* **460**, 392–395 (2009).
55. K. Hahn, M. Miranda, V. A. Francis, J. Vendrell, A. Zorzano, A. A. Teleman, PP2A regulatory subunit PP2A-B' counteracts S6K phosphorylation. *Cell Metab.* **11**, 438–444 (2010).
56. R. Habib, R. Kim, H. Neitzel, I. Demuth, K. Chrzanowska, E. Seemanova, R. Faber, M. Digweed, R. Voss, K. Jäger, K. Sperling, M. Walter, Telomere attrition and dysfunction: A potential trigger of the progeroid phenotype in nijmegen breakage syndrome. *Aging* **12**, 12342–12375 (2020).
57. T. Steenstrup, J. D. Kark, S. Verhulst, M. Thinggaard, J. V. B. Hjelmborg, C. Dalgård, K. O. Kyvik, L. Christiansen, M. Mangino, T. D. Spector, I. Petersen, M. Kimura, A. Benetos, C. Labat, R. Sinnreich, S. J. Hwang, D. Levy, S. C. Hunt, A. L. Fitzpatrick, W. Chen, G. S. Berenson, M. Barbieri, G. Paolisso, S. M. Gadalla, S. A. Savage, K. Christensen, A. I. Yashin, K. G. Arbeev, A. Aviv, Telomeres and the natural lifespan limit in humans. *Aging* **9**, 1130–1142 (2017).
58. M. J. P. Simons, Questioning causal involvement of telomeres in aging. *Ageing Res. Rev.* **24**, 191–196 (2015).
59. M. Raices, H. Maruyama, A. Dillin, J. Karlseder, Uncoupling of longevity and telomere length in *C. elegans*. *PLOS Genet.* **1**, e30 (2005).
60. Y. Jiang, J. R. Broach, Tor proteins and protein phosphatase 2A reciprocally regulate Tap42 in controlling cell growth in yeast. *EMBO J.* **18**, 2782–2792 (1999).
61. O. Medvedik, D. W. Lamming, K. D. Kim, D. A. Sinclair, MSN2 and MSN4 link calorie restriction and TOR to sirtuin-mediated lifespan extension in Saccharomyces cerevisiae. *PLoS Biol.* **5**, e261 (2007).
62. K. Demanelis, F. Jasmine, L. S. Chen, M. Chernoff, L. Tong, D. Delgado, C. Zhang, J. Shinkle, M. Sabarinathan, H. Lin, E. Ramirez, M. Oliva, S. Kim-Hellmuth, B. E. Stranger, T.-P. Lai, A. Aviv, K. G. Ardlie, F. Aguet, H. Ahsan; GTEx Consortium, J. A. Doherty, M. G. Kibriya, B. L. Pierce, Determinants of telomere length across human tissues. *Science* **369**, eaaz6876 (2020).
63. S. A. Kamranvar, X. Chen, M. G. Masucci, Telomere dysfunction and activation of alternative lengthening of telomeres in B-lymphocytes infected by Epstein-Barr virus. *Oncogene* **32**, 5522–5530 (2013).
64. J. Zhang, S. Haider, J. Baran, A. Cros, J. M. Guberman, J. Hsu, Y. Liang, L. Yao, A. Kasprzyk, BioMart: A data federation framework for large collaborative projects. *Database (Oxford)* **2011**, bar038 (2011).
65. J. Herrero, M. Muffato, K. Beal, S. Fitzgerald, L. Gordon, M. Pignatelli, A. J. Vilella, S. M. J. Searle, R. Amode, S. Brent, W. Spooner, E. Kulesha, A. Yates, P. Flicek, Ensembl comparative genomics resources. *Database* **2016**, bav096 (2016).
66. H. Wickham, *ggplot2: Elegant Graphics for Data Analysis* (Springer-Verlag, 2016).
67. G. R. Warnes, B. Bolker, L. Bonebakker, R. Gentleman, W. Huber, A. Liaw, T. Lumley, M. Maechler, A. Magnusson, S. Moeller, M. Schwartz, B. Venables, T. Galili, "gplots: Various R Programming Tools for Plotting Data" (R package version 3.1.1., 2020); https://cran.r-project.org/web/packages/gplots/index.html.
68. *ibima / tpe-old — Bitbucket* (29 August 2021); https://bitbucket.org/ibima/tpe-old/src/master/.
69. S. Campbell, The Progeria Research Foundation Cell Bank. https://www.progeriaresearch.org/cell-and-tissue-bank/, 20 July 2022.
70. D. Gerstorf, L. Bertram, U. Lindenberger, G. Pawelec, I. Demuth, E. Steinhagen-Thiessen, G. G. Wagner, Behavioural Science Section/The Berlin Aging Study II-An overview. Editorial. *Gerontology* **62**, 311–315 (2016).
71. F. Kannenberg, K. Gorzelniak, K. Jäger, M. Fobker, S. Rust, J. Repa, M. Roth, I. Björkhem, M. Walter, Characterization of cholesterol homeostasis in telomerase-immortalized Tangier disease fibroblasts reveals marked phenotype variability. *J. Biol. Chem.* **288**, 36936–36947 (2013).
72. B. Neuner, A. Lenfers, R. Kelsch, K. Jäger, N. Brüggmann, P. van der Harst, M. Walter, Telomere length is not related to established cardiovascular risk factors but does correlate with red and white blood cell counts in a german blood donor population. *PLOS ONE* **10**, e0139308 (2015).
73. R. M. Cawthon, Telomere length measurement by a novel monochrome multiplex quantitative PCR method. *Nucleic Acids Res.* **37**, e21 (2009).
74. J. B. McGuire, T. J. James, C. J. Imber, S. D. St. Peter, P. J. Friend, R. P. Taylor, Optimisation of an enzymatic method for β-galactosidase. *Clin. Chim. Acta* **326**, 123–129 (2002).
75. R. K. Gary, S. M. Kindell, Quantitative assay of senescence-associated beta-galactosidase activity in mammalian cell extracts. *Anal. Biochem.* **343**, 329–334 (2005).
76. M. López-Ratón, M. X. Rodríguez-Álvarez, C. C. Suárez, F. Gude-Sampedro, OptimalCutpoints: An R package for selecting optimal cutpoints in diagnostic tests. *J. Stat. Softw.* **61**, 1–36 (2014).
77. J. Böhringer, R. Santer, N. Schumacher, F. Gieseke, K. Cornils, M. Pechan, B. Kustermann-Kuhn, R. Handgretinger, L. Schöls, K. Harzer, I. Krägeloh-Mann, I. Müller, Enzymatic characterization of novel arylsulfatase A variants using human arylsulfatase A-deficient immortalized mesenchymal stromal cells. *Hum. Mutat.* **38**, 1511–1520 (2017).
78. Z. Darzynkiewicz, G. Juan, DNA content measurement for DNA ploidy and cell cycle analysis. *Current protocols in cytometry.* **7**, cy0705s00 (2001).
79. R Core Team, *R: A Language and Environment for Statistical Computing* (R Foundation for Statistical Computing, 2020).

Acknowledgments: We thank W. Wright and J. Shay (University of Texas Southwestern Medical Center, Dallas) for providing reagents and advice. This work would not have been possible without the positive encouragement from W. Wright. We thank M. Hanna (Mercury Medical Research and Writing), U. Kornak (University of Göttingen), and E. Steinhagen-Thiessen (Charité Berlin and University of Rostock) for proofreading the manuscript. The manuscript was edited at Springer Nature Author Services. We thank K. Tränkner (WriteNow, Berlin, Germany) for preparing the schematic drawings. We thank M. Haschke, B. Köttgen, S. Zigan, and K. Binder (Charité–Universitätsmedizin Berlin) for technical support. We thank A. del Rio (Institute of Organic Synthesis and Photoreactivity, Bologna, Italy) for providing the SIRT inhibitor (compound BCI-150). We are grateful for financial and technical support from Labor Berlin. We thank J. Reunert, T. Marquardt, and E. Orso for providing control cells. We thank also all co-PIs from the BASE-II research project (L. Bertram, D. Gerstorf, U. Lindenberger, G. Pawelec, E. Steinhagen-Thiessen, and G. G. Wagner). Support for computing equipment was provided by the European Union [EFRE (European Fund for Regional Development)]. **Funding:** This work was supported by Sonnenfeld Stiftung grant (to K.J.), European Union's Horizon 2020 research and innovation program grant 633589 (to S.M. and G.F.), German Federal Ministry of Education and Research (Bundesministerium für Bildung und Forschung, BMBF) grant 03VP06230 (to G.F.), German Federal Ministry of Education and Research (Bundesministerium für Bildung und Forschung, BMBF) grants for the BASE-II research project nos. 16SV5536K, 16SV5537, 16SV5538, 16SV5837, 01UW0808, 01GL1716A, and 01GL1716B (to I.D.), Hermann und Lilly Schilling-Stiftung für medizinische Forschung im Stifterverband (to A.He.), and Stiftung für Pathobiochemie und Molekulare Diagnostik (to M.W.). **Ethics statement:** All procedures were performed in accordance with the ethical standards of the responsible committee. The cell lines were either established with the ethical approval of the Ethics Committee of the "Ärztekammer Westfalen Lippe" and the Medical Faculty of the University of Münster (5 VI Walter), the University of Rostock (A2019-0134, A.He.; A2019-0134), and the consent of the participants or their parents (for children) or approved by the local Ethics committees of the Technische Universität Dresden (EK45022009) and the University Medical Center Rostock (A2019-0134). The HGP cell lines were a gift from the Progeria Research Foundation [L. Gordon; the PRF Cell and Tissue Bank is Institutional Review Board (IRB) approved by the Rhode Island Hospital Committee on the Protection of Human Subjects, Federal Wide Assurance FWA00001230, study CMTT#0146-09] and were collected according to the regulations of the Progeria Research Foundation. All participants from the BASE-II study gave written informed consent to the study protocol that was approved by the Ethics

Committee of the Charité-Universitätsmedizin Berlin (number of the ethical approval: EA2/029/09). **Author contributions:** Conceptualization: M.W. Methodology: K.J., J.M., S.M., B.N., K.G., S.T., I.D., A.S., M.W., F.W., C.H., A.Ha., and M.E.G. Visualization: K.J., J.M., M.E.G., S.M., and M.W. Supervision: M.W., G.F., and S.M. Writing—original draft: K.J. and M.W. Writing—review and editing: S.M., B.N., G.F., A.Ha., A.He., K.J., and M.W. **Competing interests:** The authors declare that they have no competing interests. **Data and materials availability:** All data needed to evaluate the conclusions in the paper are present in the paper and/or the Supplementary Materials and at https://doi.org/10.5281/zenodo.6477501. All program codes for the presented TPE-OLD candidate gene selection and analyses are freely available online at https://doi.org/10.5281/zenodo.6477501. Because of concerns for participant privacy, BASE-II data are available only upon reasonable request. External scientists may apply to the Steering Committee of BASE-II for data access. Please refer to the BASE-II website (www.base2.mpg.de/7549/data-documentation) for additional information. Please contact L. Müller, scientific coordinator, at lmueller@mpib-berlin.mpg.de. The progeria cell lines can be provided by the Progeria Research Foundation Inc. pending scientific review and a completed material transfer agreement. Requests for the progeria cell lines should be submitted to the Progeria Research Foundation. Both the two youngest and two oldest donors shown in fig. S19A can be provided by Coriell Institute pending scientific review and a completed material transfer agreement. Requests for the cell lines should be submitted to the Coriell Institute.

Submitted 14 October 2021
Accepted 5 July 2022
Published 17 August 2022
10.1126/sciadv.abk2814